

# A Precise Fitting Formula for Gravitational Wave Spectra from Phase Transitions

Huai-ke Guo,<sup>a</sup> Fazlollah Hajkarim,<sup>b</sup> Kuver Sinha,<sup>b</sup>  
Graham White,<sup>c</sup> Yang Xiao<sup>d,e</sup>

<sup>a</sup>International Centre for Theoretical Physics Asia-Pacific, University of Chinese Academy of Sciences, 100190 Beijing, China


<sup>b</sup>Department of Physics and Astronomy, University of Oklahoma, Norman, OK 73019, USA

<sup>c</sup>School of Physics and Astronomy, University of Southampton, Southampton SO17 1BJ, United Kingdom

<sup>d</sup>CAS Key Laboratory of Theoretical Physics, Institute of Theoretical Physics, Chinese Academy of Sciences, Beijing 100190, P. R. China

<sup>e</sup>School of Physical Sciences, University of Chinese Academy of Sciences, Beijing 100049, P. R. China

E-mail: [guohuaike@ucas.ac.cn](mailto:guohuaike@ucas.ac.cn), [fazlollah.hajkarim@ou.edu](mailto:fazlollah.hajkarim@ou.edu), [kuver.sinha@ou.edu](mailto:kuver.sinha@ou.edu),  
[g.a.white@soton.ac.uk](mailto:g.a.white@soton.ac.uk), [xiaoyang@itp.ac.cn](mailto:xiaoyang@itp.ac.cn)

**Abstract.** Obtaining a precise form for the predicted gravitational wave (GW) spectrum from a phase transition is a topic of great relevance for beyond Standard Model (BSM) physicists. Currently, the most sophisticated semi-analytic framework for estimating the dominant contribution to the spectrum is the sound shell model; however, full calculations within this framework can be computationally expensive, especially for large-scale scans. The community therefore generally manages with fit functions to the GW spectrum, the most widely used of which is a single broken power law. We provide a more precise fit function based on the sound shell model: our fit function features a double broken power law with two frequency breaks corresponding to the two characteristic length scales of the problem – inter-bubble spacing and thickness of sound shells, the second of which is neglected in the single broken power law fit. Compared to previously proposed fits, we demonstrate that our fit function more faithfully captures the GW spectrum coming from a full calculation of the sound shell model, over most of the space of the thermodynamic parameters governing the phase transition. The physical origins of the fit parameters and their dependence on the thermodynamic parameters are studied in the underlying sound shell model: in particular, we perform a series of detailed scans for these quantities over the plane of the strength of the phase transition ( $\alpha$ ) and the bubble wall velocity ( $v_w$ ). Wherever possible, we comment on the physical interpretations of these scans. The result of our study can be used to generate accurate GW spectra with our fit function, given initial inputs of  $\alpha$ ,  $v_w$ ,  $\beta/H$  (nucleation rate parameter) and  $T_n$  (nucleation temperature) for the relevant BSM scenario. 

---

## Contents

<b>1</b>	<b>Introduction</b>	<b>1</b>
<b>2</b>	<b>General Framework for First Order Phase Transition</b>	<b>3</b>
2.1	Broken Power Law Approximation	6
2.2	Double Broken Power Law Fit	7
<b>3</b>	<b>New Fit Formula</b>	<b>8</b>
<b>4</b>	<b>Physical Behavior of Fit and FOPT Parameters</b>	<b>10</b>
<b>5</b>	<b>Conclusions</b>	<b>12</b>
<b>A</b>	<b>Other Scanning Plots</b>	<b>17</b>
<b>B</b>	<b>GW Spectrum for a Specific Choice of FOPT Parameters</b>	<b>17</b>
B.1	Mathematica script	17
B.2	Python script	21

---

## 1 Introduction

One of the most plausible cosmological mechanisms for producing a stochastic gravitational wave (GW) background is a first order phase transition [1]. The most common motivation for such an epoch is electroweak symmetry breaking, which can become strongly first order in extensions to the Standard Model [2–101]. Other motivations for a cosmic first order phase transition include dark matter [35, 88, 102–112, 112–121], symmetry breaking chains from a grand unified group [25, 122–127], or the QCD transition [116–119, 128–139]. The GW spectrum resulting from a cosmological phase transition has three contributions - a term arising from the collision of scalar shells, a term arising from crashing sound waves in the plasma and the after party of turbulence. For most of the parameter space, it is widely accepted that the sound shell source produces the dominant contribution to the stochastic GW background [1].

At the present time, the most widely used semi-analytical framework for calculating the velocity spectrum sourced by sound waves is provided by the sound shell model [140]. The corresponding GW spectrum was calculated for a non-expanding Universe in [141], and subsequently extended to an expanding Universe in [142]. Alongside the semi-analytical framework, simulations have recently also made great progress in this area [143–145] and motivate the use of a broken power law for the GW spectrum, which has been adopted by the LISA cosmology working group [1]. The single broken power law comes from the simplifying assumption of ignoring the details of the velocity profile of the sound waves, and instead taking the RMS<sup>1</sup> of the fluid velocity,  $U_f$ ; the peak frequency is then set by the mean bubble separation [146]. On the other hand, recent work with the sound shell model [147, 148] motivates using a double broken power law, which comes from including the full velocity profile. The use of the full velocity profile results in qualitatively different physics:

---

<sup>1</sup>Root mean square.

the spectrum is better described by a double broken power law since the velocity profile now contains information about the thickness of the profile, which implies that there is more than one physically significant scale.

It should be noted that the dependence of the spectral features of a fit on the underlying thermodynamic parameters of the phase transition (the nucleation temperature  $T_n$ , nucleation rate parameter  $\beta$ , phase transition strength  $\alpha$ , and wall speed  $v_w$ ) is a difficult question and progress can be made by a combination of analytical calculations and numerical fits. In principle, one could imagine the possibility of reconstructing the values of four thermal parameters from a hypothetical spectrum [147], (though a more conservative study argued for three [149]). Such a wealth of information, if it were to be available, would render GW detectors almost competitive with colliders in the extent of details of the underlying model they can reveal [79]. In a sense, the community is actually already in the era where the degree of precision we use in calculating GW spectra becomes important, since LIGO currently puts constraints on the Pati-Salam unification scenario [150]. This urgency will grow as next generation detectors cover many more decades in frequency at a much high strain sensitivity (for a review see [151]). From a beyond Standard Model (BSM) physicist’s point of view, the ideal workflow would be the following: for every point on the parameter space of the model, obtain the thermodynamic parameters  $(T_n, \beta, \alpha, v_w)$ , and compute the GW spectrum using the sound shell model (or better still, use actual simulations); then check how the parameter space is constrained by GW detectors. Needless to say, full calculations of the sound shell model, not to speak of actual simulations, are difficult and expensive; to perform large-scale scans over the parameter space of particle physics models and obtain the predicted GW spectrum, portable and simple fits to the spectrum, and the interpretation of the fit parameters, become necessary.

The main purpose of this paper is to provide such a precise fit function. Elaborating further, our goal in the current paper will be the following: given a particle physics model with input values of  $(T_n, \beta, \alpha, v_w)$ , an appropriate fit function for the GW spectrum is provided, along with a public code. A historical progression of fit functions can help contextualize our results: the cornerstone of GW phenomenology has been a broken power law with a peak set by the mean bubble separation; this was recently improved upon by the double broken power law fit function introduced in [147, 148] with fit parameters corresponding to the peak amplitude, two frequency breaks and the spectral slope between them; our fit function is a further improvement, by introducing an extra parameter that governs the IR behavior of the spectrum. Scanning over  $(\alpha, v_w)$ , we show that our fit function reproduces, much more faithfully, the GW spectrum coming from the sound shell model (Fig. 2). We provide data files and scripts in `Python` and `Mathematica` that can be directly used by a front-end user to generate accurate GW spectra, given inputs of  $(T_n, \beta, \alpha, v_w)$  for a given beyond-SM scenario. This tool is expected to allow the community to fully investigate the extent to which each individual BSM model can be constrained by future detectors, without actually performing calculations with the sound shell model.

The second purpose of our paper is to attempt to study the physical interpretation of the fit parameters by way of detailed scans on the plane of  $(\alpha, v_w)$ . We provide scans over  $(\alpha, v_w)$  in the deflagration, hybrid, and detonation regimes and study the velocity and enthalpy profiles, as well as a host of quantities: the maximum velocity  $v_{max}$ , the thermal efficiency factor  $\kappa$ , the peak frequency  $f_p$ , the maximum relic density  $\Omega_p$ , the width of the velocity profile  $\delta_\xi$ , and the fit parameters  $\tilde{b}$  and  $\tilde{a}$ . The dependence of these quantities on  $(\alpha, v_w)$  can be highly non-linear. Wherever possible, we make qualitative statements about

this dependence, as well as correlations with the relative behaviour of other parameters.

This paper is organized as follows. In Section 2, we discuss the general framework for the calculation of GWs in a first order phase transition and show, in turn, the standard broken power law approximation (Section 2.1) and the improved double broken power law fit (Section 2.2). In Section 3 we introduce our new fit function and discuss its faithfulness in capturing the GW spectrum compared to the older fits. The dependence of various physical and fit parameters on  $(\alpha, v_w)$  is discussed in Section 4, where we also display the results of our scans. Discussions and code for using the new fit function <sup>2</sup> are relegated to the Appendix A and B. Finally we summarize and conclude in Section 5.

## 2 General Framework for First Order Phase Transition

In this section we briefly review the framework for the calculation of GWs from sound waves during a first order phase transition (FOPT) [140–142, 147, 152–158]. The details of a gravitational wave spectrum produced by sound waves depend upon a number of macroscopic features of the phase transition. For instance, it matters how far apart the bubbles are during the phase transition, how fast the bubbles expand, the fraction of energy released during the phase transition that is dumped into kinetic energy modes, the details of the fluid velocity and of course the temperature at which all this occurs.

Since the background is expanding, the key parameter for describing the nucleation of bubbles during the phase transition is not the nucleation rate - as the phase transition always begins when the nucleation rate is fast enough so that the nucleation of bubbles can keep pace with the expanding Universe. Instead, it is customary to consider how fast the nucleation rate increases from this bare minimum rate

$$\Gamma \sim e^{-S(t)} \sim e^{-S_0 + \beta(t-t_n)} \quad (2.1)$$

where  $t_n$  is the time of nucleation at  $S_0$  is the value needed to have at least one bubble per hubble volume. Unless there is a significant amount of supercooling [150], it is  $\beta$  that actually controls the time scale of the transition. It is straightforward to relate this parameter to the mean bubble separation [141, 147],  $R_*$

$$\frac{\beta}{H_n} = (8\pi)^{\frac{1}{3}} \frac{v_w}{r_*}. \quad (2.2)$$

Here, the wall velocity is denoted by  $v_w$  and

$$r_* = H_n R_*, \quad (2.3)$$

where  $H_n$  is the Hubble rate at the nucleation time. The fraction of the kinetic energy dumped into the plasma, as well as the details of the velocity profile tend to depend upon how strong the transition is. This is governed by the change in the trace anomaly,  $\Delta\theta$  in the energy momentum tensor between the phases, normalized to the enthalpy of the symmetric phase,  $w_s$ ,

$$\alpha = \frac{4}{3} \frac{\Delta\theta}{w_s} \Big|_{T=T_n}. \quad (2.4)$$

Making predictions in the sound shell model require solving the hydrodynamic equations and using the macroscopic thermal parameters of a phase transition as boundary conditions. We

---

<sup>2</sup>It can be downloaded from this [GitHub link](#).

use a bag model to match solutions of thermodynamic variables at the boundary between the two phases. We consider a non-vanishing bag constant, which we denote as  $\epsilon$ , [159] which has the value

$$\alpha = \frac{4}{3} \frac{\epsilon}{w_n}. \quad (2.5)$$

There are three qualitatively distinct types of phase transitions which are delineated by the value of the bubble wall velocity, compared to the Jouget velocity,  $v_j$  and the speed of sound,  $c_s$  [141, 146, 160]. Specifically, the Jouget velocity is defined as

$$c_J = c_s \frac{\left(1 + \sqrt{\alpha(2 + 3\alpha)}\right)}{(1 + \alpha)}, \quad (2.6)$$

where the detonation regime occurs when  $v_w > c_J > c_s$ , a deflagration of subsonic regime is when  $v_w < c_J < c_s$ . A hybrid transition involves both deflagration and detonation phases. Initially,  $v_w < c_s$  and  $v_w < c_J$  indicating a deflagration. However, as the phase transition evolves, energy accumulates in the bubble wall or in a shock front preceding the wall, potentially allowing the bubble to accelerate to a velocity  $v_w$  such that  $c_s < v_w < c_J$  or even  $v_w > c_J$ , at which point a detonation may occur [141, 146, 160].

The relative density of GW for each value of  $z = kR_*$  corresponding to a specific frequency  $k = 2\pi f$  is controlled by the kinetic energy fraction  $K$ , as well as [141, 147] the lifetime of the soundshell source,  $H_n \tau_v$  and its characteristic scale,  $H_n R_*$ , for which we use the shorthand

$$J = H_n R_* H_n \tau_v = r_* \left(1 - \frac{1}{\sqrt{1 + 2x}}\right) \equiv r_* \Upsilon, \quad (2.7)$$

where  $x = H_n R_* / \sqrt{K}$  and  $r_*$  defined in Eq. (2.3). We can then write the gravitaitonal wave power spectrum at the time it is produced as,

$$\Omega_{\text{GW}}(z) = 3K^2(v_w, \alpha) J \frac{z^3}{2\pi^2} \tilde{P}_{\text{GW}}(z). \quad (2.8)$$

If one takes the RMS fluid velocity, rather than calculating the gravitational wave spectrum from the full velocity profile, one can write the frequency dependent analytical form of spectral density  $z^3 \tilde{P}_{\text{GW}}$  for GW from Refs. [146, 161] as a broken power law

$$S_{\text{SW}}(f) = \left(\frac{f}{f_{\text{SW}}}\right)^3 \left[\frac{7}{4 + 3(f/f_{\text{SW}})^2}\right]^{7/2}. \quad (2.9)$$

We will be comparing the predictions of the soundshell model to this single broken power law throughout, as this simplified case is ubiquitous in the literature.

In such a case we take the kinetic energy fraction as  $K = \Gamma \bar{U}_f^2$  where  $\Gamma = \bar{w}/\bar{v}$  is the ratio of the average enthalpy to the average fluid velocity. Further, the mean squared velocity defines [141, 162]

$$\bar{U}_f^2 = \frac{3}{\bar{w}v_w^3} \int w \xi^2 \frac{v^2}{1 - v^2} d\xi \quad (2.10)$$

that can be approximated  $\bar{U}_f \approx \sqrt{\frac{3}{4} \frac{\kappa \alpha}{1 + \alpha}}$  and the quantity  $\kappa$  is given by [141]

$$\kappa = \frac{3}{\epsilon w^3} \int d\xi \xi^2 w^2 \gamma^2 v^2. \quad (2.11)$$

where we have defined

$$\xi \equiv r/t, \quad (2.12)$$

with  $r$  being the distance from the center of the bubble and  $t$  being the time from the onset of the phase transition and nucleation.

The sound shell model differs from the results of numerical simulations as some sound shells collide before they reach a self similar solution, that is a solution that depends upon the ratio  $\xi = r/t$  only. The effect of this was numerically approximated in Ref. [147] by introducing an error factor

$$\Omega_{\text{GW}}(z) = \Omega_{\text{GW}}^{\text{SSM}}(z)\Sigma(v_w, \alpha), \quad (2.13)$$

where  $\Omega_{\text{GW}}^{\text{SSM}}(z)$  is the relic from sound wave model at redshift  $z$  and  $\Sigma(v_w, \alpha)$  compensates from the sound shell model's overestimation of the gravitational waves due to energy lost into vorticity modes as demonstrated in Ref. [163]. As the precise nature of this factor for all possible thermal parameters is not known, we assume it as  $\Sigma(v_w, \alpha) = 1$  in order to focus on other aspects of sound shell model that affect the GW signal. The reader should note that it is a simple fix to include the results of Ref. [163] if one is working in a regime where interpolations of their result can be used.

After formation the power spectra will redshift like radiation leading to its dilution and a shift in the peak frequency such that,

$$\Omega_{\text{GW}}^0(f) = F_{\text{GW}}^0 \Omega_{\text{GW}}(z(f)), \quad (2.14)$$

where the  $F_{\text{GW}}^0$  factor that redshifts the GW relic from its moment of production in the early Universe to today is

$$F_{\text{GW}}^0 = \Omega_{\gamma,0} \left( \frac{g_{*s,0}}{g_{*s}} \right)^{\frac{4}{3}} \frac{g_*}{g_{*,0}} \simeq (3.57 \pm 0.05) \times 10^{-5} \left( \frac{100}{g_*} \right)^{\frac{1}{3}}, \quad (2.15)$$

assuming  $g_* \simeq g_{*s}$  at  $T \gg T_\nu$ . The peak frequency is set by the mean bubble separation and a redshift factor

$$f = \frac{z}{r_*} f_{*,0}, \quad (2.16)$$

where  $z = kR_*$  and the redshift factor is given by

$$f_{*,0} = 2.6 \times 10^{-6} \text{ Hz} \left( \frac{T_n}{100 \text{ GeV}} \right) \left( \frac{g_*}{100} \right)^{\frac{1}{6}}. \quad (2.17)$$

Here we use the degrees of freedom of the thermal background of SM particles for energy density  $g_*$  and entropy density  $g_{*s}$  from Ref. [164].

Putting everything together, the relic density of GW from sound waves is given by [142, 146]

$$\Omega_{\text{GW}} h^2 \simeq 1.2 \times 10^{-6} \left( \frac{100}{g_*} \right)^{1/3} K^2 \Upsilon \left( \frac{H_n}{\beta} \right) v_w S_{\text{SW}}(f). \quad (2.18)$$

The low frequency tail of the GW spectrum from sound waves can either have  $k^3$  or  $k^9$  dependence based on recent studies [165–167]. We will address this issue in the future.

## 2.1 Broken Power Law Approximation

If the velocity profile is replaced with the RMS fluid velocity, there is a single scale left in the mean bubble separation. Thus under this approximation, the gravitational wave power spectrum is a broken power law (BPL) with a peak set by the mean bubble separation. This approximation has been the cornerstone of gravitational wave phenomenology and we will briefly review it here, following Ref. [155]. The peak amplitude is set by a thermal efficiency factor, which ref [155] develop an analytic approximation for,

$$\kappa(\alpha, v_w) \equiv \begin{cases} v_w^{6/5} \frac{6.9\alpha}{1.36 - 0.037\sqrt{\alpha+\alpha}}, & 0 \lesssim v_w \lesssim 0.2, \\ \frac{\alpha^{2/5}}{0.017 + (0.997 + \alpha)^{2/5}}, & 0.2 \lesssim v_w \lesssim 0.8, \\ \frac{\alpha}{0.73 + 0.083\sqrt{\alpha+\alpha}}, & 0.8 \lesssim v_w \lesssim 1. \end{cases} \quad (2.19)$$

In the above we have given (very) rough limits of validity of each expression with approximate values of  $v_w$ . The peak frequency of the spectrum is given by

$$f_p^{\text{BPL}} = 1.19 \times 10^{-6} \frac{1}{v_w} \left( \frac{g_*}{100} \right)^{1/6} \left( \frac{T}{100} \right) \times 0.7 \times \frac{\beta}{H_n}, \quad (2.20)$$

with the mean bubble separation being the only scale in the problem

$$R_* = (8\pi)^{1/3} \frac{\beta}{v_w}. \quad (2.21)$$

The peak assuming adiabatic index  $\Gamma \approx 4/3$  is then set in our approximation mostly by the RMS fluid velocity [146]

$$\Omega_p^{\text{BPL}} \approx 1.2 \times 10^{-6} \left( \frac{100}{g_*} \right)^{1/3} \left( \frac{4}{3} \right)^2 \bar{U}_f(\alpha, v_w)^4 \frac{H_n}{\beta} v_w \Upsilon, \quad (2.22)$$

which can be related to the thermal efficiency factor and trace anomaly,

$$\bar{U}_f \approx \sqrt{\frac{3}{4} \kappa(\alpha, v_w) \alpha}. \quad (2.23)$$

The approximation can be rather poor. In Fig. 1, we show a comparison of the GW relic density coming from the full sound shell model and that calculated using the broken power law given by Eq. (2.22). The left (right) panel of the first row shows the ratio of the peak relic densities (frequencies) as a function of  $v_w$  for several fixed values of  $\alpha$ . The second row depicts the same quantities as a function of  $\alpha$ , for several fixed values of  $v_w$ . There are two metrics of comparison to keep track of. Firstly, it is clear that  $\Omega_p/\Omega_p^{\text{BPL}} \sim 1$  and  $f_p/f_p^{\text{BPL}} \sim 1$  is only achieved for a narrow range of values of  $\{v_w, \alpha\}$ . For example, from the top and bottom left panels, it is clear that  $\Omega_p/\Omega_p^{\text{BPL}} \sim 1$  is achieved for  $\alpha \sim 0.2 - 0.4$  with  $v_w \sim 0.4$ . Similarly, from the top and bottom right panels, it is clear that  $0.1 \lesssim f_p/f_p^{\text{BPL}} \lesssim 1$  is achieved for  $v_w \lesssim 0.3$  and for  $f_p/f_p^{\text{BPL}} \sim 0.3$  for  $v_w \gtrsim 0.9$  while being relatively stable across values of  $\alpha$ .

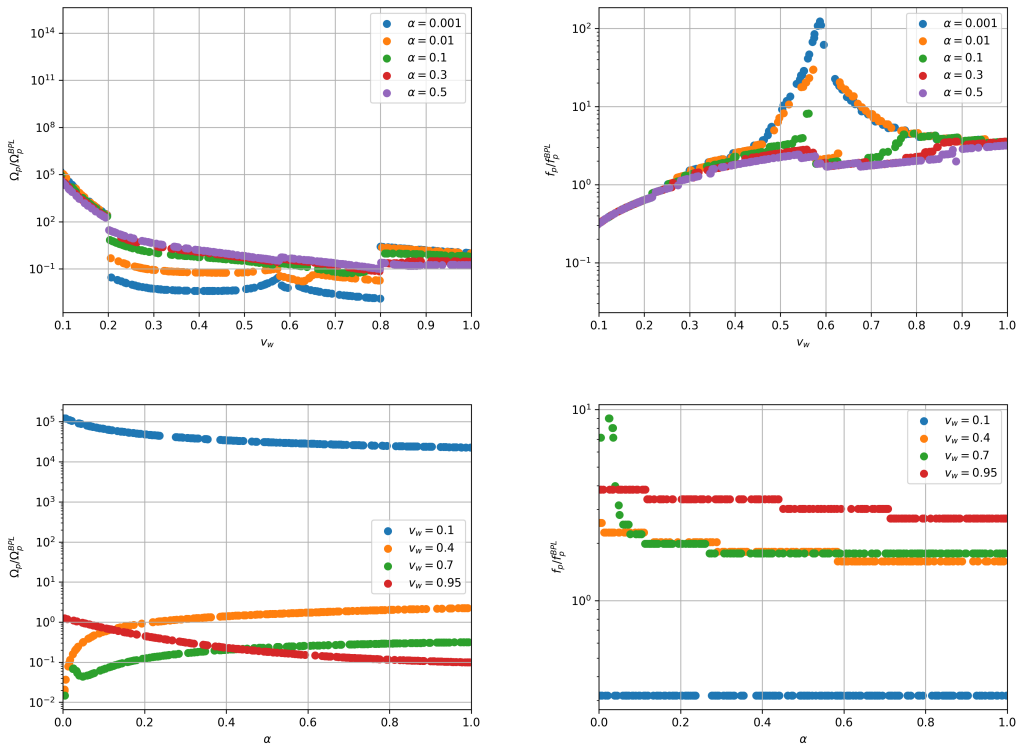


**Figure 1.** Ratio of  $\Omega_p/\Omega_p^{\text{BPL}}$  and  $f_p/f_p^{\text{BPL}}$  in different cases of either fixed  $\alpha$ 's or  $v_w$ 's. For the definition of  $\Omega_p^{\text{BPL}}$  see Eq. (2.22).

## 2.2 Double Broken Power Law Fit

Using the full velocity profile in calculating the gravitational wave spectrum (re)introduces a second scale, the thickness of the sound shell. A double broken power law fit function to match the calculated GW spectrum was therefore introduced in Refs. [147, 148]

$$\Omega_{\text{GW,fit}} = F_{\text{GW}}^0 \Omega_p M(s, r_b, b), \quad (2.24)$$

Here,  $\Omega_p$  is the peak value of the GW relic density, and the corresponding frequency is  $f_p$ . Also,  $F_{\text{GW}}^0$  is determined in Eq. (2.15). The parameter  $r_b = f_b/f_p$  gives the ratio between the two breaks in the spectrum. The parameter  $b$  gives the spectral slope between the two breaks. The variable  $s = f/f_p$  is introduced to normalize the frequency with respect to the peak frequency. The function  $M$  is given by [141, 147, 148]

$$M(s, r_b, b) = s^9 \left( \frac{1 + r_b^4}{r_b^4 + s^4} \right)^{(9-b)/4} \left( \frac{b + 4}{b + 4 - m + ms^2} \right)^{(b+4)/2}, \quad (2.25)$$

where the choice of  $m$  ensures that for  $r_b < 1$  one gets a peak at  $s = 1$  and  $M(1, r_b, b) = 1$ . This leads to

$$m = (9r_b^4 + b) / (r_b^4 + 1). \quad (2.26)$$

In our work, when using the fit formula from [147] we use PySwarm optimization package to determine  $b$  and  $r_b$ . We consider a range of values for  $b$  and  $r_b$ :  $b \in [-200, 200]$  and  $r_b \in [0, 200]$ .



### 3 New Fit Formula

We will find that the fit function Eq. 2.25 described in the previous Section gives a poor approximation when calculating the acoustic contribution to the gravitational wave spectrum where the hydrodynamic equations are solved using a non-vanishing bag constant  $\epsilon$ . However, physically we still expect a doubly broken power law to work. We therefore, consider the following new fit function that is different from [147]

$$\Omega_{\text{GW}}h^2 = \Omega_p \cdot \left(\frac{f}{\tilde{s}_0}\right)^9 \cdot \frac{(2 + \tilde{r}_b^{-12+\tilde{b}})}{\left[\left(\frac{f}{\tilde{s}_0}\right)^{\tilde{a}} + \left(\frac{f}{\tilde{s}_0}\right)^{\tilde{b}} + \tilde{r}_b^{-12+\tilde{b}} \cdot \left(\frac{f}{\tilde{s}_0}\right)^{12}\right]}. \quad (3.1)$$

Here the parameters  $\Omega_p$ ,  $\tilde{s}_0$ ,  $\tilde{a}$ ,  $\tilde{b}$  and  $\tilde{r}_b = f_b/f_p$  are calculated by fitting to the numerical solution to the GW spectrum. The parameter,  $\tilde{r}_b$  controls the ratio between the peaks,  $\tilde{b}$  adjusts the spectral slope between the two breaks in the frequency, while  $\tilde{a}$  governs the IR behavior of the GW spectrum. It should be noted that the two spectral breaks correspond to the two characteristic length scales in the system: the peak frequency  $f_p$  corresponds to the mean bubble separation  $R_*$ , while the frequency  $f_b$  corresponds to the thickness of the sound shell  $\Delta R_*$ . Compared to the fit formula in Eq. 2.25, an extra parameter  $\tilde{a}$  has been introduced. The values of all parameters in Eq. 3.1 are produced from our calculations of the GW relic density based on the sound shell model [141, 147, 148]. The dependence of the fit parameters on the underlying physical parameters such as  $\alpha$  and  $v_w$  governing the phase transition are explored in Section 4.

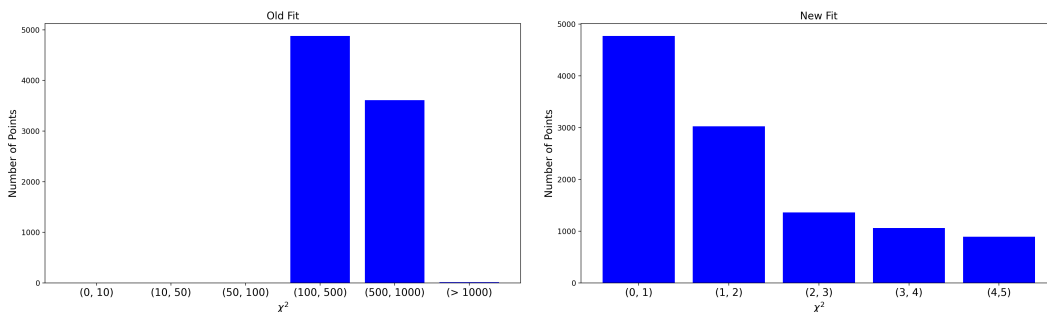


**Figure 2.** Histogram for comparison of fits using the fit function in Eq. (2.24) motivated by Ref. [141, 147, 148] and our proposed fit formula in Eq. (3.1).

Before proceeding to compare the different fit formulas, we pause to give details about our computation procedure. A Monte Carlo approach to fitting Eq. 3.1 to the GW spectrum of the sound shell model is adopted. Relevant variables  $\Omega_p$ ,  $\tilde{s}_0$ ,  $\tilde{a}$ ,  $\tilde{b}$  and  $\tilde{r}_b$  are first initialized. Our algorithm then executes a loop 100,000 times, each iteration randomly generating the parameters introduced in Eq. 3.1 to match the GW spectrum from the sound shell model data. The appropriateness of the fit is measured by calculating residuals - the squared differences between the logarithms of actual data for  $\Omega_{\text{GW}}h^2$  and the predictions from Eq. 3.1. The program continually updates the parameters that result in the lowest residuals, storing the best-fit parameters. After completing all iterations, it uses these parameters to generate the final predicted model values and calculates the total error between this fit model and the original sound shell data. The objective is to robustly determine the parameters that

best explain how the GW spectrum behaves across various frequencies, optimizing the fit to minimize error.

A comparison of the fit to GW spectrum from [141] as given by Eq. 2.24 to our new fit in Eq. 3.1 is illuminating. We do a  $\chi^2$  analysis based on the fit equations and the GW spectrum produced by the sound shell model, using the full bubble velocity profile based on [141, 142]. The two histograms in Fig. 2 show the results.

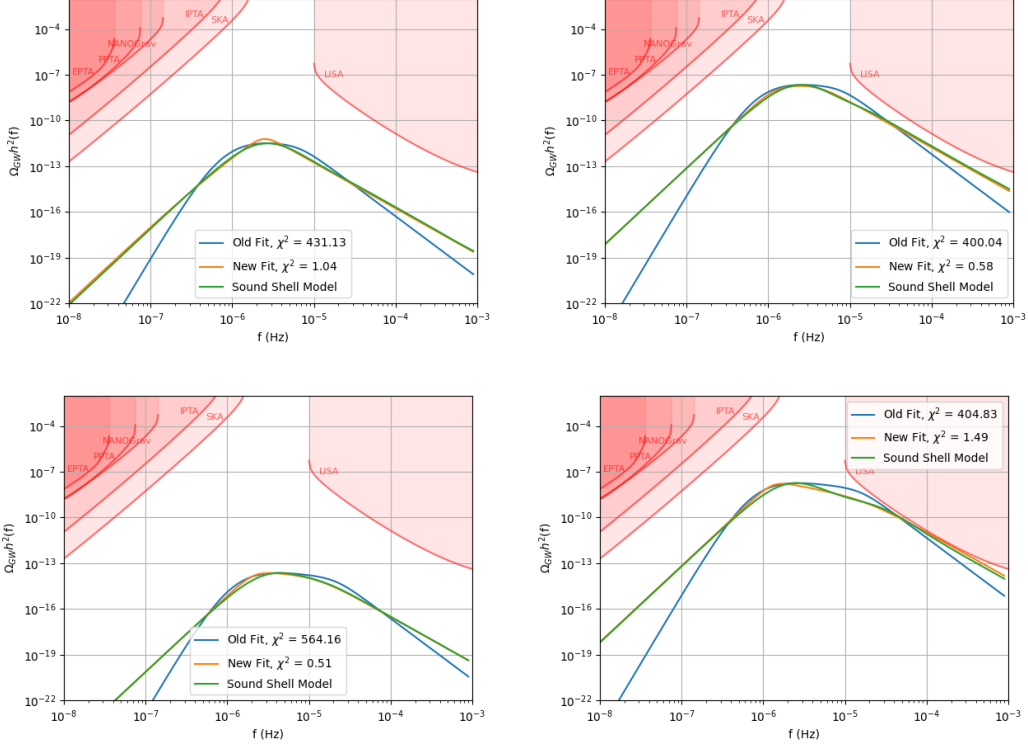


**Figure 3.** A benchmark point of GW from FOPT showing the relic density of GW with respect to frequency for “old fit” ([147]), “new fit” (the current work), and sound shell model ([141, 147, 148]) is plotted. Various current and future observational constraints are also shown and labeled using the integrated sensitivity curves from [168] for different experiments. Here we assume  $T_n = 100$  GeV and  $\beta/H = 1$ .

As can be seen from the left panel of Fig. 2, the  $\chi^2$  values for Eq. 2.24 are much larger than one and most values are above a hundred. On the other hand, the right panel of Fig. 2 shows that most data points have  $\chi^2$  values smaller than one for the new fit function in Eq. 3.1 introduced in this paper. While some data points do have  $\chi^2$  large than one, the number of such points decreases as  $\chi^2$  increases. In Fig. 3, we consider four benchmark points and show the  $\chi^2$  values for the old and new fits in each panel. These benchmarks have these set of FOPT parameters:  $[6.13 \times 10^{-2}, 3.08 \times 10^{-3}, 1, 100]$ ,  $[1.28 \times 10^{-1}, 8.66 \times 10^{-2}, 1, 100]$ ,  $[3.32 \times 10^{-1}, 6.36 \times 10^{-2}, 1, 100]$  and  $[5.99 \times 10^{-1}, 3.47 \times 10^{-1}, 1, 100]$  for this FOPT parameters  $[v_w, \alpha, \beta/H, T_n(\text{GeV})]$ . For these benchmarks it is apparent that the new fit in Eq. 3.1 matches better with the sound shell model than the fit formula in Eq. 2.24. Overall, based on these figures, we have validated the quality of the fit function for most choices of  $v_w$  and  $\alpha$ . This implies that our proposed fit in Eq. 3.1 more accurately captures the features of GW spectrum

from the sound shell model and can be used by the community (see Appendix B for the fit function code).

#### 4 Physical Behavior of Fit and FOPT Parameters

Having demonstrated the appropriateness of our fit function, we proceed towards a deeper physical understanding of the different parameters that we have introduced. We perform a scan over the following input parameters: the wall velocity  $v_w$  and the strength of transition  $\alpha$ , keeping the nucleation temperature  $T_n = 100$  GeV and the bubble nucleation rate  $\beta/H = 1$  fixed. Using these parameters, we calculate: (i) the maximum velocity  $v_{\max}$ , (ii) the width of velocity profile  $\delta_\xi$  (defined as the width of the velocity profile in a window 95 % of  $v_{\max}$ ), (iii) the corresponding value of  $\xi$  as  $\xi_{\max}$ , and (iv) the difference between the values of the enthalpy before the wall and after it i.e.  $\delta_w$ . Our results are displayed in Figs. 4 - 8 (also see Appendix A for more scanning plots).

We begin with a discussion of Fig. 4. Here, we depict values of  $\tilde{r}_b$  (top panel),  $\tilde{b}$  (middle panel), and  $\tilde{a}$  (bottom panel) on the plane of  $\{v_w, \alpha\}$  for three regimes: deflagration (red), detonation (green) and hybrid (blue). The value of  $\alpha$  is chosen to vary from  $10^{-3} - 1$ , since we are interested in studying the global behavior of the parameters. For the plot of  $\tilde{r}_b$ , it is clear that there is some structure: for example, in the deflagration regime, the values of  $\tilde{r}_b$  for a given  $\alpha$  are small at small values of  $v_w$ , increase around  $v_w \sim 0.2 - 0.4$ , before decreasing again. Similarly, in the detonation regime, the values of  $\tilde{r}_b$  for a given value of  $v_w$  decrease with increasing  $\alpha$ . A somewhat opposite behavior can be discerned in the hybrid regime, where increasing  $\alpha$  corresponds to lower  $\tilde{r}_b$ . In contrast to the results for  $\tilde{r}_b$ , it is difficult to discern any structure in the scans of  $\tilde{b}$  and  $\tilde{a}$ . It is therefore fruitful to study the dependencies in a series of two dimensional plots, which we turn to next.

In Fig. 5, we show the velocity and enthalpy profiles with respect to  $\xi$  for different choices of  $\alpha$ . The scan has been performed over different values of wall velocity  $0 < v_w < 1$ . The velocity and enthalpy profiles exhibit the behavior expected for the deflagration, hybrid, and detonation regimes, respectively [79]. In the deflagration mode, the plasma in front of the bubble wall flows outward while remaining static inside the bubble. The velocity profiles to the left of the maximum in all panels of Fig. 5 exhibit this behavior. As  $v(\xi)$  increases, a discontinuity appears and  $v(\xi) \rightarrow 0$ ; this is the shock front, beyond which a supersonic deflagration (hybrid) mode develops when the velocity exceeds the sound speed. The value of  $\alpha$  determines the maximum value of  $v_{\max}$  and maximum of  $w_{\max}$  where the velocity profile maximises over different values of  $\xi$ . Each value of  $v_{\max}$  occurs when  $\xi = v_w$ .

Fig. 6 depicts the behavior of the various physical quantities, as well as the fit parameters, as a function of  $v_w$  for several benchmark values of  $\alpha = 0.001, 0.01, 0.1, 0.3$ , and  $0.5$ . The behaviour of  $v_{\max}$  w.r.t.  $v_w$  is shown in the bottom left panel of Fig. 6. It reaches a maximum that depends on the value  $\alpha$ ; a similar pattern is exhibited by the thermal efficiency factor  $\kappa$  defined in Eq. 2.11 and depicted in the top right panel. The results of this panel, as well as the top right panel depicting  $\kappa$ , are consistent with the left panels of Fig. 5. The peak frequency  $f_p$  is depicted in the bottom right panel of Fig. 6 and shows a local maximum where  $v_{\max}$  is maximized. The dependence of  $\Omega_p$  w.r.t.  $v_w$  is shown in the second row of the left panel of Fig. 6.  $\Omega_p$  is a decreasing function of  $v_w$  in the deflagration regime; on reaching  $v_{\max}$ , it rises somewhat and then continues falling in the hybrid and detonation regimes. We have defined the width of velocity profile  $\delta_\xi$  as the difference between the values of  $\xi$  when  $\xi_{\max} = v_w$  and  $v(\xi_{\text{width}}) = 0.95 v_{\max}$ . This quantity is shown in the left panel of the first

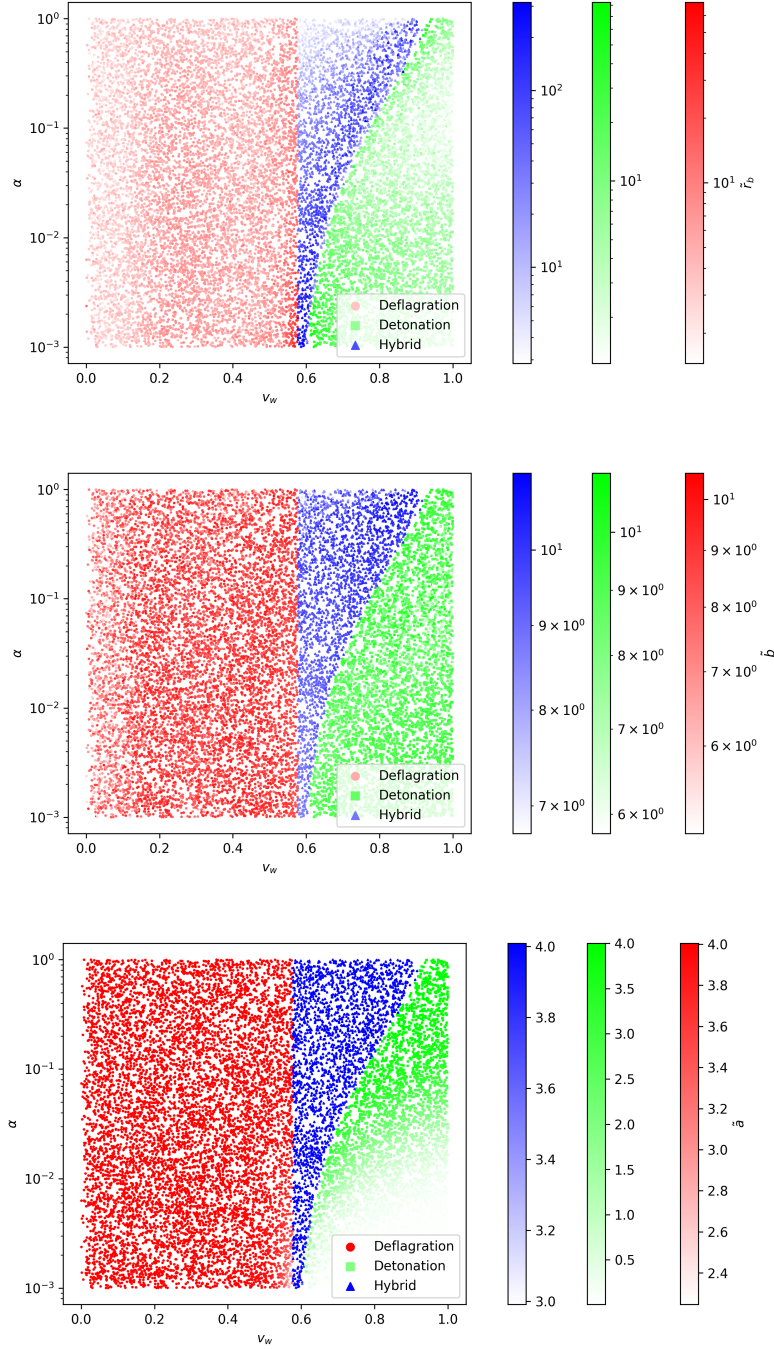


**Figure 4.** From top to bottom: scatter plots for  $v_w$ ,  $\alpha$  and  $\tilde{r}_b$ ; for  $v_w$ ,  $\alpha$  and  $\tilde{b}$ ; and for  $v_w$ ,  $\alpha$  and  $\tilde{a}$ , respectively. The type of FOPT is shown in the legend. Here we assume  $T_n = 100$  GeV and  $\beta/H = 1$ .

row. Its behavior matches with expectations from the velocity profiles shown in Fig. 5. The value of  $\xi_{\max}$  increases monotonously with  $v_w$ , independently of  $\alpha$ , as shown in the right of panel of the fourth row of Fig. 6.

We now turn to a discussion of the fit parameters  $\tilde{b}$  and  $\tilde{a}$ . Firstly, it should be noted that

smaller values of  $\tilde{b}$  correspond to a situation where more energy resides in the contribution from the thickness of the sound shell rather than from the bubble separation. Conversely, larger values of  $\tilde{b}$  correspond to more energy residing in the contribution from the bubble separation. While it is difficult to discern structure, we do find a linearly increasing trend in  $\tilde{b}$  as  $v_w$  increases, shown by trend lines, albeit crude. Physically, it is reasonable that as  $v_w$  increases, more energy should reside in the bubble separation contribution. The behavior of the fit parameter  $\tilde{a}$  in the left panel of the third row is interesting. It should be noted that smaller values of  $\tilde{a}$  correspond to sharper IR spectra, while larger values of  $\tilde{a}$  correspond to shallower IR spectra. It is clear that the value of  $\tilde{a}$  is insensitive to variations in  $v_w$  in the deflagration mode, but swiftly decreases after  $v_{\max}$ , for all values of  $\alpha$ .

We now turn to a discussion of Fig. 8, where a scan over  $\alpha$  between 0 and 1 for fixed values of  $v_w = 0.1, 0.4, 0.7, 0.95$  was performed. The plot of the  $\tilde{a}$  parameter versus  $\alpha$  is shown in the fourth row, left panel.  $\tilde{a}$  appears to be constant with a value of around 4, which reduces when it reaches the maximum of  $v_{\max}$ . This is consistent with the behavior in Fig. 6. The plot of  $\tilde{b}$  versus  $\alpha$  is shown in the second row of the right panel of Fig. 7. It is difficult to discern a specific pattern here; nevertheless, we have made a crude linear fit. For  $v_w = 0.1, 0.4$ , and  $0.7$ , we see that  $\tilde{b}$  decreases very mildly with increasing  $\alpha$ .

## 5 Conclusions

The sound shell model currently provides the most sophisticated semi-analytical framework for calculating the GW spectrum in models of BSM physics. In conjunction with numerical simulations, a precision GW spectrum frontier is then already somewhat within reach for particle physicists; one can then ask why fit functions of the type studied in this paper are even necessary, or why the physical interpretation of fit parameters is an interesting question. The response is that full calculations of the sound shell model, not to speak of actual simulations, are difficult and expensive; to perform large-scale scans over the parameter space of particle physics models and obtain the predicted GW spectrum, portable and simple fits to the spectrum, and the interpretation of the fit parameters, become necessary. Providing such a fit – currently the one that most faithfully captures the full results coming from the sound shell model – has been the goal of this paper. We have shared the results of our work in a set of `CSV`, `Python` and `Mathematica` files<sup>3</sup>. These files can be used by the BSM community to efficiently depict the GW spectrum at various points in the parameter space of their models.

Studies in GW physics are rapidly entering a precision frontier. Indeed, as pointed out by a subset of the present authors in [158], uncertainties of several orders of magnitude can be introduced in the calculation of the GW spectrum if one neglects careful treatments of the source lifetime; mean bubble separation; employing a beyond the bag model approximation when solving the hydrodynamics equations and explicitly calculating the fraction of energy in the fluid from these equations rather than using a fit. The incorporation of these effects constitutes, currently, the “highest level of diligence” (in the parlance of [158]) in obtaining the GW spectrum. Calculating the full GW spectrum at the highest level of diligence, and providing the relevant fit functions, constitute concrete future directions.

---

<sup>3</sup>[GitHub link](#).

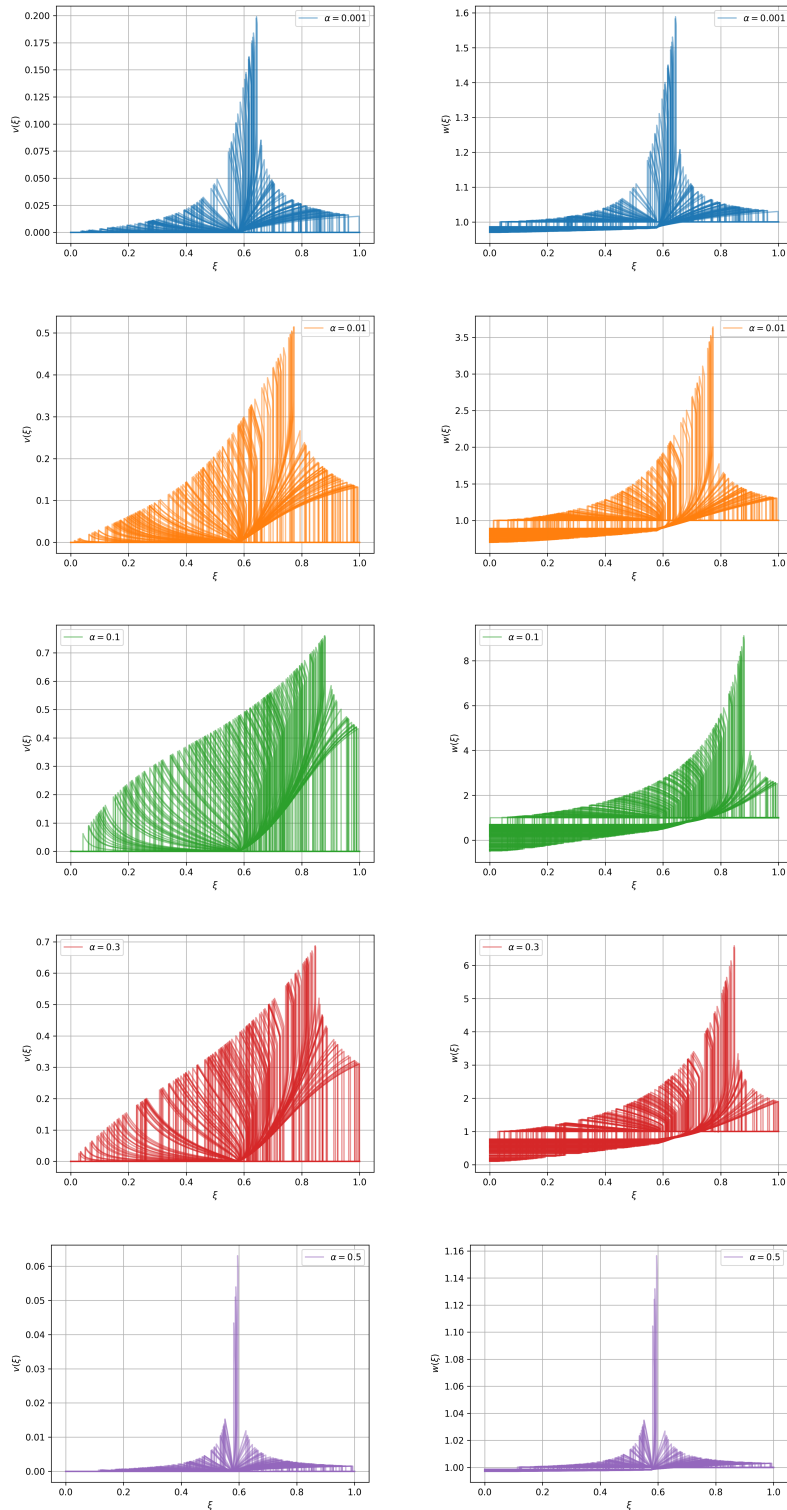


**Figure 5.** Velocity and enthalpy profiles for fixed values of  $\alpha$ . Each row of these panels corresponds to a color that are blue, orange, green, red and violet equivalent to a specific value of  $\alpha = 0.001, 0.01, 0.1, 0.3, 0.5$  shown in the legends.

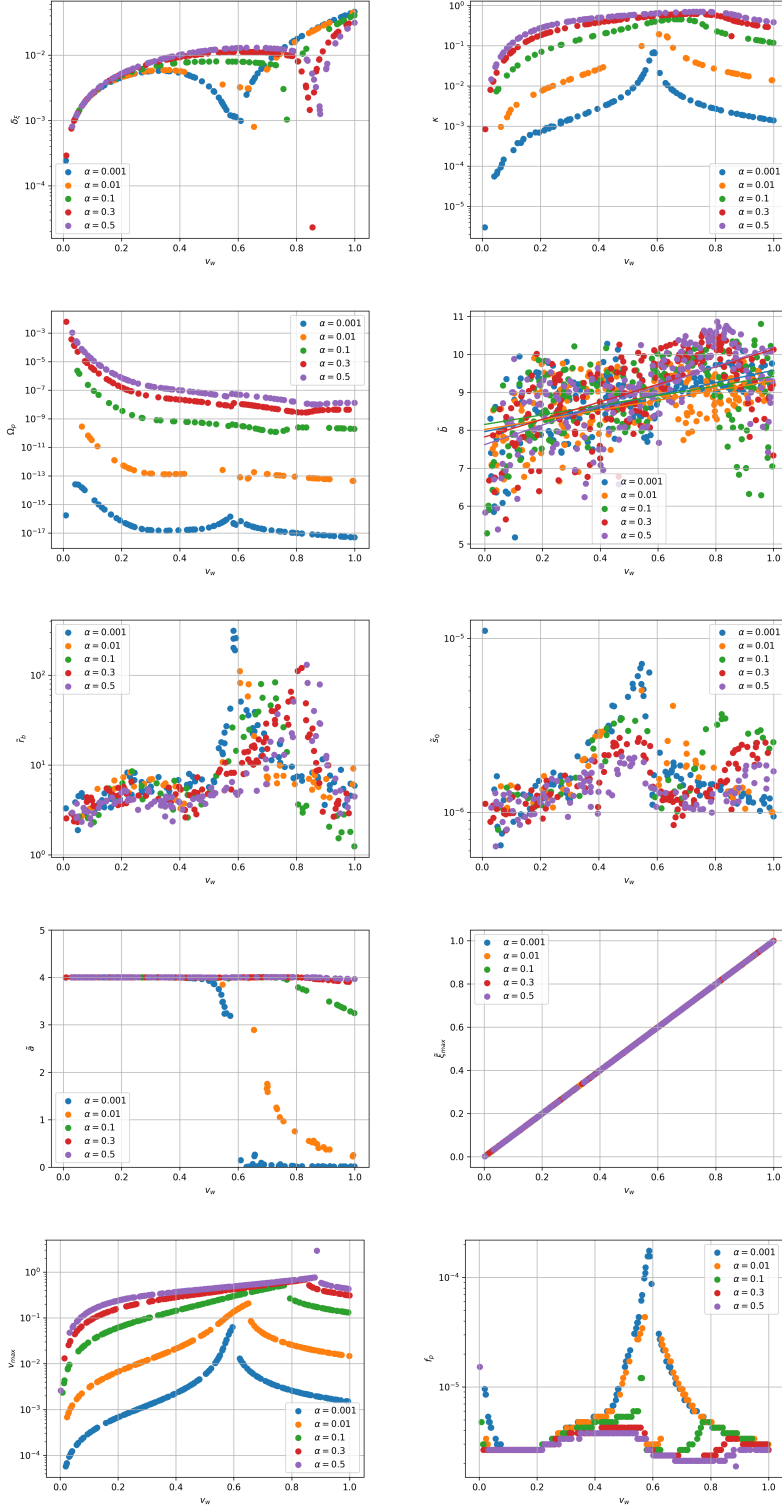


**Figure 6.** Plots for different variables with respect to  $\alpha$  for fixed  $\alpha$ 's are shown. Each of colors blue, orange, green, red and violet corresponds to a specific value of  $\alpha = 0.001, 0.01, 0.1, 0.3, 0.5$  shown in the legends. We describe them in the main text. Here we assume  $T_n = 100$  GeV and  $\beta/H = 1$ .

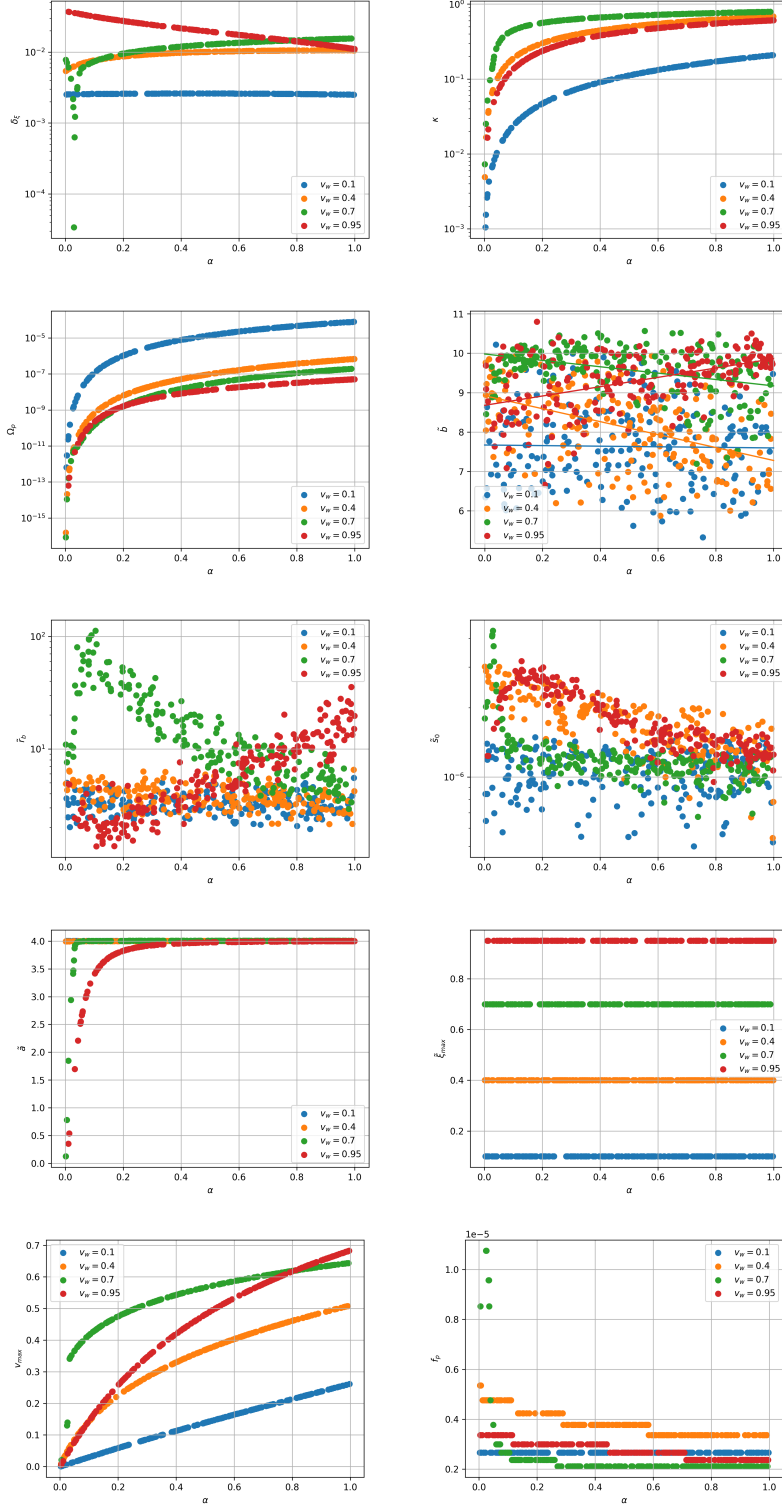


**Figure 7.** Plots for different variables with respect to  $\alpha$  for fixed  $v_w$ 's are shown. Each of colors blue, orange, green and red corresponds to a specific value of  $v_w = 0.1, 0.4, 0.7, 0.95$ . We describe them in the main text. Here we assume  $T_n = 100$  GeV and  $\beta/H = 1$ .



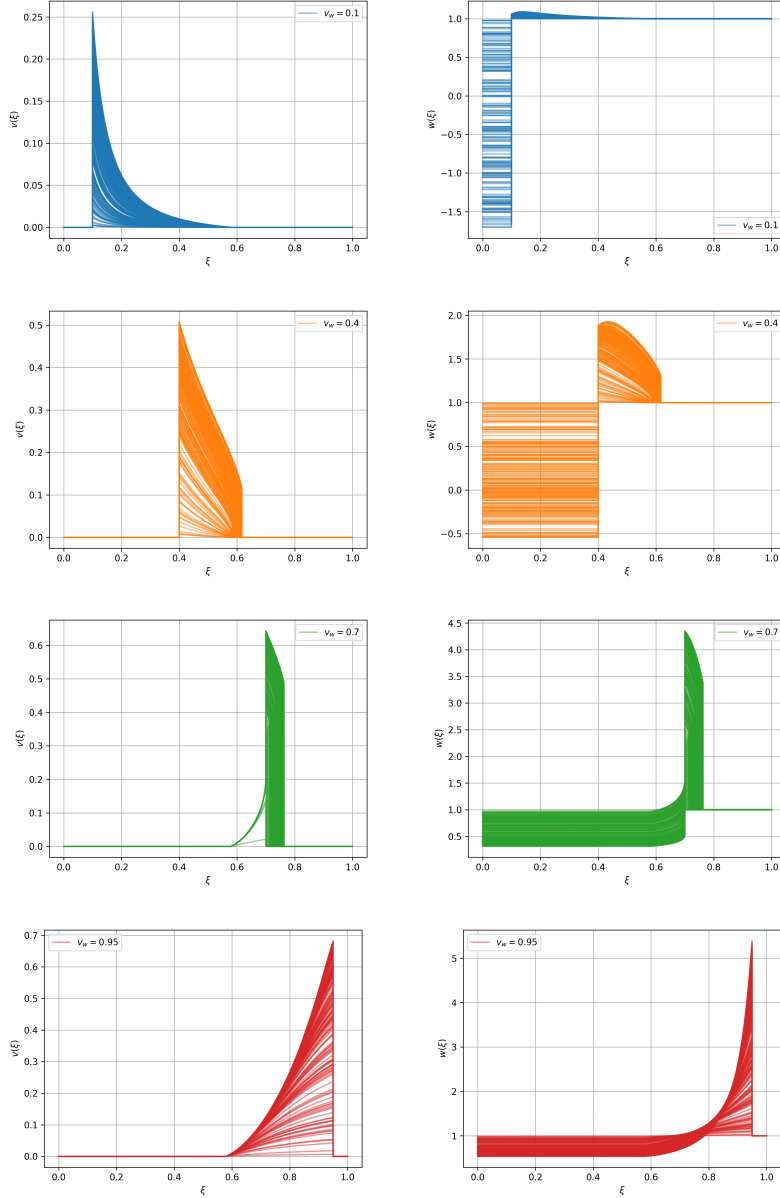


**Figure 8.** Velocity and enthalpy profiles for fixed values of wall velocity  $v_w$ . Each row of these panels corresponds to a color that are blue, orange, green and red equivalent to a specific value of  $v_w = 0.1, 0.4, 0.7, 0.95$  shown in the legends.

The precision GW frontier has several other challenges that lie outside the scope of this work. The transitions between the different power law regimes in the GW spectrum, the existence of new regimes, the shape of the GW spectrum near the peak, and the peak frequency depend on several factors: fluctuations in the local temperature affect the distribution of nucleated bubbles [169]; energy lost to vorticity can suppress the spectrum [163]; and dissipative effects encoded by the shear viscosity, bulk viscosity, and thermal conduction can also suppress the spectrum [170]. Calculating these effects would make further material progress on the precision frontier.

## Acknowledgments

We are grateful to Jose Miguel No for collaboration during the initial stages of the project, and to Daniel Vagie for useful discussions. F.H. and K.S. thank the organizers of the Mitchell Conference in May 2024 at Texas A & M University for their hospitality and support during the final stages of this project. They are also grateful to the organizers of workshop of Center for Theoretical Underground Physics and Related Areas (CETUP\* - 2024), The Institute for Underground Science at Sanford Underground Research Facility (SURF), Lead, South Dakota for their hospitality and financial support. K.S. would like to thank the Aspen Center for Theoretical Physics, supported by the National Science Foundation grant PHY-2210452, for hospitality during the course of this work.

## A Other Scanning Plots

We have shown other scanning plots over  $\delta_\xi$  and  $\kappa$  parameter space in this section in Fig. 9. We also represented the variation of some of our new fit parameters:  $\tilde{r}_b$ ,  $\tilde{b}$  and  $\tilde{a}$  as introduced in Eq (3.1). In first panel we have shown the plot for  $\tilde{r}_b$  i.e. the ratio of frequencies between two peaks. As Fig. 9 shows large values of  $\tilde{r}_b$  are accumulating between  $0 \lesssim \delta_\xi \lesssim 0.01$  and  $10^{-2} \lesssim \kappa \lesssim 0.5$  for all regimes and  $\tilde{r}_b$  decreases as  $\delta_\xi$  and  $\kappa$  are changing from these regions. Also, the second panel shows the changes parameter  $\tilde{b}$  w.r.t.  $\delta_\xi$  and  $\kappa$ . For deflagration and hybrid regimes increasing  $\delta_\xi$  and  $\kappa$  makes  $\tilde{b}$  larger. However, for the detonation regime  $\tilde{b}$  slightly reduces by decreasing of  $\kappa$ . In the last panel we examine the variation of parameter  $\tilde{a}$  that deviates from 4 depending on the values of  $\delta_\xi$  and  $\kappa$ . As it can be seen the points in deflagration and hybrid regimes are almost independent of  $\delta_\xi$  and  $\kappa$ . However, as  $\kappa$  increases  $\tilde{a}$  also increases for detonation regime.

## B GW Spectrum for a Specific Choice of FOPT Paramters

Here we briefly explain how one can use our script to calculate the spectrum of GW from sound waves of FOPT. We provide two scripts written in Python and Mathematica.

### B.1 Mathematica script

The Mathematica script is displayed below:

```
1 (*Load the CSV file*)
2 data = Import[NotebookDirectory[] <> "data-fopt-fit.csv"];
3
4 (*Extract and clean column names from the first row*)
5 columnNames = StringTrim /@ First[data];
6
7 (*Remove the header row to isolate the data*)
8 data = Rest[data];
9
10 (*Print column names to check*)
11 Print[columnNames];
12
13 (*Assign each column to a separate variable using safe access to \
14 Position*)
15 vw = If[Length[Position[columnNames, "vw"]] > 0,
16   data[[All, Position[columnNames, "vw"][[1, 1]]], {}];
17 alpha = If[Length[Position[columnNames, "alpha"]] > 0,
```

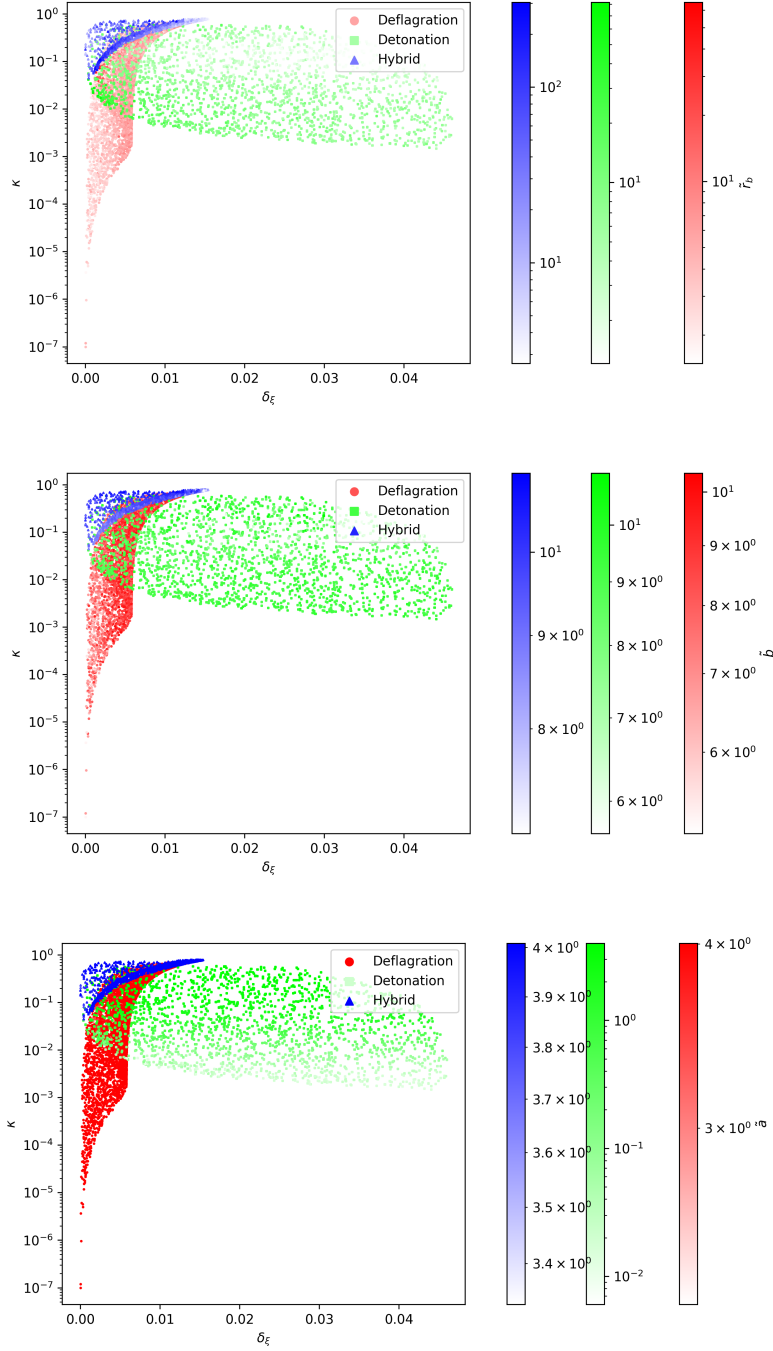


**Figure 9.** From top to bottom: scatter plots for  $\delta_\xi$ ,  $\kappa$  and  $\tilde{r}_b$ ; for  $\delta_\xi$ ,  $\kappa$  and  $\tilde{b}$ ; and for  $\delta_\xi$ ,  $\kappa$  and  $\tilde{a}$ . The type of FOPT is shown in the legend. Here we assume  $T_n = 100$  GeV and  $\beta/H = 1$ .

```

18 data[[All, Position[columnNames, "alpha"][[1, 1]]], {}];
19 betaH = If[Length[Position[columnNames, "betaH"]] > 0,
20 data[[All, Position[columnNames, "betaH"][[1, 1]]], {}];
21 Tn = If[Length[Position[columnNames, "Tn"]] > 0,
22 data[[All, Position[columnNames, "Tn"][[1, 1]]], {}];

```

```

23 fp = If[Length[Position[columnNames, "f_p"]] > 0,
24   data[[All, Position[columnNames, "f_p"][[1, 1]]], {}];
25 Omp = If[Length[Position[columnNames, "Om_p"]] > 0,
26   data[[All, Position[columnNames, "Om_p"][[1, 1]]], {}];
27 at = If[Length[Position[columnNames, "at"]] > 0,
28   data[[All, Position[columnNames, "at"][[1, 1]]], {}];
29 bt = If[Length[Position[columnNames, "bt"]] > 0,
30   data[[All, Position[columnNames, "bt"][[1, 1]]], {}];
31 rbt = If[Length[Position[columnNames, "rbt"]] > 0,
32   data[[All, Position[columnNames, "rbt"][[1, 1]]], {}];
33 s0t = If[Length[Position[columnNames, "s0t"]] > 0,
34   data[[All, Position[columnNames, "s0t"][[1, 1]]], {}];
35 omega0t =
36   If[Length[Position[columnNames, "omega_0t"]] > 0,
37     data[[All, Position[columnNames, "omega_0t"][[1, 1]]], {}];
38 K = If[Length[Position[columnNames, "K"]] > 0,
39   data[[All, Position[columnNames, "K"][[1, 1]]], {}];
40
41 (*Define the data points*)
42 dataVWAlphaFP = Transpose[{vw, alpha, fp}];
43 dataVWAlphaOmP = Transpose[{vw, alpha, Omp}];
44 dataVWAlphaAt = Transpose[{vw, alpha, at}];
45 dataVWAlphaBt = Transpose[{vw, alpha, bt}];
46 dataVWAlphaRbt = Transpose[{vw, alpha, rbt}];
47 dataVWAlphaS0t = Transpose[{vw, alpha, s0t}];
48 dataVWAlphaOmega0t = Transpose[{vw, alpha, omega0t}];
49 dataVWAlphaK = Transpose[{vw, alpha, K}];
50
51
52 (*Create interpolating functions*)
53 intFP = Interpolation[dataVWAlphaFP, InterpolationOrder -> 1];
54 intOmP = Interpolation[dataVWAlphaOmP, InterpolationOrder -> 1];
55 intAt = Interpolation[dataVWAlphaAt, InterpolationOrder -> 1];
56 intBt = Interpolation[dataVWAlphaBt, InterpolationOrder -> 1];
57 intRbt = Interpolation[dataVWAlphaRbt, InterpolationOrder -> 1];
58 intS0t = Interpolation[dataVWAlphaS0t, InterpolationOrder -> 1];
59 intOmega0t =
60   Interpolation[dataVWAlphaOmega0t, InterpolationOrder -> 1];
61 intK = Interpolation[dataVWAlphaK, InterpolationOrder -> 1];
62
63 (*Evaluate at a point*)
64 vw0 = 0.5;
65 alpha0 = 0.5;
66 fp0 = intFP[vw0, alpha0];
67 at0 = intAt[vw0, alpha0];
68 bt0 = intBt[vw0, alpha0];
69 rbt0 = intRbt[vw0, alpha0];
70 s0t0 = intS0t[vw0, alpha0];
71 Omegap0 = intOmega0t[vw0, alpha0];
72 K0 = intK[vw0, alpha0];
73
74 (*Degrees of freedom*)
75 gstarData = Import[NotebookDirectory[] <> "gstar.txt", "Table"];
76 gHighTemp = {{1.*10^14*gstarData[[1, 1]], gstarData[[1, 2]]}};
77 dataG1 = Join[gHighTemp, gstarData];
78 TData = dataG1[[All, 1]];
79 gstarData = dataG1[[All, 2]];
80 gstarFun = Interpolation[Transpose[{TData, gstarData}]];

```

```

81
82 (*Frequency domain*)
83 fdomainDefault = 10^Range[-24, 24, 48/999] // N;
84
85 (*Generating fit parameters from the interpolated function*)
86 fb0 = rbt0*fp0;
87 (*This part can be modified based on different nucleation \
88 temperatures and bubble nucleation rates.*)
89 betaHDefault = 1;
90 betaHNew = 10;
91 TnDefault = 100;
92 TnNew = 1000;
93
94 rstarDefault = (8 \[Pi])^(1/3)*vw0/betaHDefault;
95 rstarNew = (8 \[Pi])^(1/3)*vw0/betaHNew;
96 gstarDefault = gstarFun[TnDefault];
97 gstarNew = gstarFun[TnNew];
98
99 xDefault = rstarDefault/(K0^(1/2));
100 JDefault = rstarDefault*(1 - 1/(1 + 2*xDefault)^(1/2));
101 FgwDefault = 3.57*10^-5*(100/gstarDefault)^(1/3);
102 xNew = rstarNew/(K0^(1/2));
103 JNew = rstarNew*(1 - 1/(1 + 2*xNew)^(1/2));
104 FgwNew = 3.57*10^-5*(100/gstarNew)^(1/3);
105
106 f0Default = 2.6*10^-6*(TnDefault/100)*(gstarDefault/100)^(1/6);
107 kR = fdomainDefault*(rstarDefault/f0Default);
108
109
110 (*GW spectrum-default*)
111 omegaFitDefault =
112   Omegap0*(fdomainDefault/
113     s0t0)^9*((2 +
114       rbt0^(-12 + bt0))/((fdomainDefault/s0t0)^
115         at0 + (fdomainDefault/s0t0)^bt0 +
116         rbt0^(-12 + bt0)*(fdomainDefault/s0t0)^12)); // Quiet
117
118
119
120 f0New = 2.6*10^-6*(TnNew/100)*(gstarNew/100)^(1/6);
121 fdomainNew = kR/(rstarNew/f0New);
122 omegaFitNew = (omegaFitDefault/(FgwDefault*JDefault))*(FgwNew*JNew);
123
124
125 (*Plotting*)
126 ListLogLogPlot[{Transpose[{fdomainDefault, omegaFitDefault}],
127   Transpose[{fdomainNew, omegaFitNew}]},
128   PlotRange -> {{1.*10^-12, 1.*10^4}, {1.*10^-22, 1.*10^-2}},
129   Frame -> True,
130   FrameLabel -> {"f (Hz)",
131     "\!\(\*SubscriptBox[\(\[CapitalOmega]\), \
132 \(\GW\)]\)\)\!\(\*SuperscriptBox[\(\h\), \(\{2\}\)]\)"},
133   PlotLabel -> "FOPT - GW", GridLines -> Automatic, Joined -> True,
134   PlotLegends -> {"Tn = 100 GeV, beta/H = 1",
135     "Tn = 1000 GeV, beta/H = 10"}, FrameStyle -> 18, ImageSize -> 800]

```

Listing 1. Mathematica code to calculate the spectrum of GW from sound waves of FOPT.

## B.2 Python script

We have written the following code in Python to calculate GW from the phase transitions:

```
1 # Python script for this manuscript
2 import numpy as np
3 from scipy.interpolate import LinearNDInterpolator
4 from scipy.interpolate import interp1d
5 import matplotlib.pyplot as plt
6 import pandas as pd
7
8 # Load the CSV file into a DataFrame
9 df = pd.read_csv('data-fopt-fit.csv')
10
11 # Assign each column to a separate variable
12 vw = df['vw'].to_numpy()
13 alpha = df['alpha'].to_numpy()
14 betaH = df['betaH'].to_numpy()
15 Tn = df['Tn'].to_numpy()
16 f_p = df['f_p'].to_numpy()
17 Om_p = df['Om_p'].to_numpy()
18 at = df['at'].to_numpy()
19 bt = df['bt'].to_numpy()
20 rbt = df['rbt'].to_numpy()
21 s0t = df['s0t'].to_numpy()
22 omega_0t = df['omega_0t'].to_numpy()
23 K = df['K'].to_numpy()
24
25 # Interpolatoin over data (t : tilde)
26 int_f_p = LinearNDInterpolator(list(zip(vw, alpha)), f_p)
27 int_Om_p = LinearNDInterpolator(list(zip(vw, alpha)), Om_p)
28 int_at = LinearNDInterpolator(list(zip(vw, alpha)), at)
29 int_bt = LinearNDInterpolator(list(zip(vw, alpha)), bt)
30 int_rbt = LinearNDInterpolator(list(zip(vw, alpha)), rbt)
31 int_s0t = LinearNDInterpolator(list(zip(vw, alpha)), s0t)
32 int_omega_0t = LinearNDInterpolator(list(zip(vw, alpha)), omega_0t)
33 int_K = LinearNDInterpolator(list(zip(vw, alpha)), K)
34
35 vw0 = 0.5
36 alpha0 = 0.5
37
38 # Generatng fit parameters from the interpolated function
39 f_p0 = int_f_p(vw0, alpha0)
40 at0 = int_at(vw0, alpha0)
41 bt0 = int_bt(vw0, alpha0)
42 rbt0 = int_rbt(vw0, alpha0)
43 s0t0 = int_s0t(vw0, alpha0)
44 omega_p0 = int_omega_0t(vw0, alpha0)
45 K0 = int_K(vw0, alpha0)
46
47 # Degrees of freedom
48 # arXiv: https://arxiv.org/pdf/1503.03513
49 filename = "gstar.txt"
50 data_g = np.loadtxt(filename, skiprows=0)
51 g_high_temp = np.array([[1.e14 * data_g[0, 0], data_g[0, 1]]])
52 data_g1 = np.concatenate((g_high_temp, data_g))
53 T_data = data_g1[:, 0] # [GeV]
54 gstar_data = data_g1[:, 1] # [GeV]
55 gstar_fun = interp1d(T_data, gstar_data)
```

```

56 #
57 f_b0 = rbt0 * f_p0
58 # This part can be modified based on different nucleation temperatures and
    bubble nucleation rates.
59 # beta over H
60 betaH_default = 1
61 betaH_new = 10
62 # Nucleation temperature
63 Tn_default = 100 # GeV
64 Tn_new = 1000 # GeV
65 #
66 rstar_default = (8*np.pi)**(1/3)*vw0/betaH_default
67 rstar_new = (8*np.pi)**(1/3)*vw0/betaH_new
68 # Degrees of Freedom
69 gstar_default = gstar_fun(Tn_default)
70 gstar_new = gstar_fun(Tn_new)
71 #
72 x_default = rstar_default/(K0**(1/2))
73 J_default = rstar_default*(1-1/(1+2*x_default)**(1/2))
74 Fgw_default = 3.57*1e-5*(100/gstar_default)**(1/3)
75 x_new = rstar_new/(K0**(1/2))
76 J_new = rstar_new*(1-1/(1+2*x_new)**(1/2))
77 Fgw_new = 3.57*1e-5*(100/gstar_new)**(1/3)
78
79 # Frequency
80 fdomain_default = 10*np.linspace(-24,24,1000)
81
82 f0_default = 2.6*1.e-6*(Tn_default/100)*(gstar_default/100)**(1/6)
83 omega_p0_default = omega_p0
84 kR = fdomain_default * (rstar_default/f0_default)
85
86 # GW spectrum - default
87 omega_fit_default = omega_p0_default * (fdomain_default/s0t0)**9 * (
88     (2 + rbt0**(-12 + bt0)) /
89     ((fdomain_default/s0t0)**at0 + (fdomain_default/s0t0)**bt0 +
90     rbt0**(-12 + bt0) * (fdomain_default/s0t0)**12))
91
92 f0_new = 2.6*1.e-6*(Tn_new/100)*(gstar_new/100)**(1/6)
93 fdomain_new = kR / (rstar_new/f0_new)
94 omega_fit_new = (omega_fit_default / (Fgw_default*J_default)) * (Fgw_new*
    J_new)
95
96
97 # Plotting
98 plt.figure(figsize=(10, 6))
99 plt.loglog(fdomain_default, omega_fit_default, label='FOPT - Sound Waves - GW
    - $T_n = 100$ GeV and $\beta/H = 1$')
100 plt.loglog(fdomain_new, omega_fit_new, label='FOPT - Sound Waves - GW')
101
102 # Set limits for frequency and GW relic axes
103 plt.xlim(1.e-12, 1.e4)
104 plt.ylim(1.e-22, 1.e-2)
105 plt.legend()
106 plt.xlabel('f (Hz)')
107 plt.ylabel('$\Omega_{GW}h^2(f)$')
108 plt.grid(True)

```

Listing 2. Python code to calculate the spectrum of GW from sound waves of FOPT.

Using the above script and the files provided along with this paper one can generate the predicted GW spectrum by inserting the input parameters from a beyond Standard Model scenario and the cosmological scale that the phase transition occurs at. These input parameters are  $\alpha$ ,  $v_w$ ,  $\beta/H$  and  $T_n$ : with these, one can produce the GW spectrum from the above Python and Mathematica scripts <sup>4</sup>.

## References

- [1] C. Caprini et al., *Detecting gravitational waves from cosmological phase transitions with LISA: an update*, *JCAP* **03** (2020) 024 [[1910.13125](#)].
- [2] R. Caldwell et al., *Detection of early-universe gravitational-wave signatures and fundamental physics*, *Gen. Rel. Grav.* **54** (2022) 156 [[2203.07972](#)].
- [3] A. Alves, D. Gonçalves, T. Ghosh, H.-K. Guo and K. Sinha, *Di-Higgs Production in the 4b Channel and Gravitational Wave Complementarity*, *JHEP* **03** (2020) 053 [[1909.05268](#)].
- [4] G. C. Dorsch, S. J. Huber and J. M. No, *A strong electroweak phase transition in the 2HDM after LHC8*, *JHEP* **10** (2013) 029 [[1305.6610](#)].
- [5] P. Basler, M. Krause, M. Muhlleitner, J. Wittbrodt and A. Wlotzka, *Strong First Order Electroweak Phase Transition in the CP-Conserving 2HDM Revisited*, *JHEP* **02** (2017) 121 [[1612.04086](#)].
- [6] G. C. Dorsch, S. J. Huber, K. Mimasu and J. M. No, *Hierarchical versus degenerate 2HDM: The LHC run 1 legacy at the onset of run 2*, *Phys. Rev. D* **93** (2016) 115033 [[1601.04545](#)].
- [7] G. C. Dorsch, S. J. Huber, T. Konstandin and J. M. No, *A Second Higgs Doublet in the Early Universe: Baryogenesis and Gravitational Waves*, *JCAP* **05** (2017) 052 [[1611.05874](#)].
- [8] J. Bernon, L. Bian and Y. Jiang, *A new insight into the phase transition in the early Universe with two Higgs doublets*, *JHEP* **05** (2018) 151 [[1712.08430](#)].
- [9] G. C. Dorsch, S. J. Huber, K. Mimasu and J. M. No, *The Higgs Vacuum Uplifted: Revisiting the Electroweak Phase Transition with a Second Higgs Doublet*, *JHEP* **12** (2017) 086 [[1705.09186](#)].
- [10] J. O. Andersen, T. Gorda, A. Helset, L. Niemi, T. V. I. Tenkanen, A. Tranberg et al., *Nonperturbative Analysis of the Electroweak Phase Transition in the Two Higgs Doublet Model*, *Phys. Rev. Lett.* **121** (2018) 191802 [[1711.09849](#)].
- [11] K. Kainulainen, V. Keus, L. Niemi, K. Rummukainen, T. V. I. Tenkanen and V. Vaskonen, *On the validity of perturbative studies of the electroweak phase transition in the Two Higgs Doublet model*, *JHEP* **06** (2019) 075 [[1904.01329](#)].
- [12] X. Wang, F. P. Huang and X. Zhang, *Gravitational wave and collider signals in complex two-Higgs doublet model with dynamical CP-violation at finite temperature*, *Phys. Rev. D* **101** (2020) 015015 [[1909.02978](#)].
- [13] W. Su, A. G. Williams and M. Zhang, *Strong first order electroweak phase transition in 2HDM confronting future Z & Higgs factories*, *JHEP* **04** (2021) 219 [[2011.04540](#)].
- [14] H. Davoudiasl, I. M. Lewis and M. Sullivan, *Multi-TeV signals of baryogenesis in a Higgs troika model*, *Phys. Rev. D* **104** (2021) 015024 [[2103.12089](#)].

---

<sup>4</sup>[GitHub link](#).



- [15] T. Biekötter, S. Heinemeyer, J. M. No, M. O. Olea and G. Weiglein, *Fate of electroweak symmetry in the early Universe: Non-restoration and trapped vacua in the N2HDM*, *JCAP* **06** (2021) 018 [[2103.12707](#)].
- [16] Z. Zhang, C. Cai, X.-M. Jiang, Y.-L. Tang, Z.-H. Yu and H.-H. Zhang, *Phase transition gravitational waves from pseudo-Nambu-Goldstone dark matter and two Higgs doublets*, *JHEP* **05** (2021) 160 [[2102.01588](#)].
- [17] M. Aoki, T. Komatsu and H. Shibuya, *Possibility of a multi-step electroweak phase transition in the two-Higgs doublet models*, *PTEP* **2022** (2022) 063B05 [[2106.03439](#)].
- [18] D. Gonçalves, A. Kaladharan and Y. Wu, *Electroweak phase transition in the 2HDM: Collider and gravitational wave complementarity*, *Phys. Rev. D* **105** (2022) 095041 [[2108.05356](#)].
- [19] V. Q. Phong, N. M. Anh and H. N. Long, *Dual electroweak phase transition in the two-Higgs-doublet model with the S3 discrete symmetry*, *Phys. Rev. D* **107** (2023) 035020 [[2209.14672](#)].
- [20] T. Biekötter, S. Heinemeyer, J. M. No, M. O. Olea-Romacho and G. Weiglein, *The trap in the early Universe: impact on the interplay between gravitational waves and LHC physics in the 2HDM*, *JCAP* **03** (2023) 031 [[2208.14466](#)].
- [21] Anisha, L. Biermann, C. Englert and M. Mühlleitner, *Two Higgs doublets, effective interactions and a strong first-order electroweak phase transition*, *JHEP* **08** (2022) 091 [[2204.06966](#)].
- [22] O. Atkinson, M. Black, C. Englert, A. Lenz, A. Rusov and J. Wynne, *The flavourful present and future of 2HDMs at the collider energy frontier*, *JHEP* **11** (2022) 139 [[2202.08807](#)].
- [23] T. Biekötter, S. Heinemeyer, J. M. No, K. Radchenko, M. O. O. Romacho and G. Weiglein, *First shot of the smoking gun: probing the electroweak phase transition in the 2HDM with novel searches for  $A \rightarrow ZH$  in  $\ell^+\ell^-t\bar{t}$  and  $\nu b\bar{b}$  final states*, *JHEP* **01** (2024) 107 [[2309.17431](#)].
- [24] D. Gonçalves, A. Kaladharan and Y. Wu, *Gravitational waves, bubble profile, and baryon asymmetry in the complex 2HDM*, *Phys. Rev. D* **108** (2023) 075010 [[2307.03224](#)].
- [25] L. Gráf, S. Jana, A. Kaladharan and S. Saad, *Gravitational wave imprints of left-right symmetric model with minimal Higgs sector*, *JCAP* **05** (2022) 003 [[2112.12041](#)].
- [26] G. Arcadi, N. Benincasa, A. Djouadi and K. Kannike, *Two-Higgs-doublet-plus-pseudoscalar model: Collider, dark matter, and gravitational wave signals*, *Phys. Rev. D* **108** (2023) 055010 [[2212.14788](#)].
- [27] N. Blinov, S. Profumo and T. Stefaniak, *The Electroweak Phase Transition in the Inert Doublet Model*, *JCAP* **07** (2015) 028 [[1504.05949](#)].
- [28] F. P. Huang and J.-H. Yu, *Exploring inert dark matter blind spots with gravitational wave signatures*, *Phys. Rev. D* **98** (2018) 095022 [[1704.04201](#)].
- [29] A. Paul, B. Banerjee and D. Majumdar, *Gravitational wave signatures from an extended inert doublet dark matter model*, *JCAP* **10** (2019) 062 [[1908.00829](#)].
- [30] S. Fabian, F. Goertz and Y. Jiang, *Dark matter and nature of electroweak phase transition with an inert doublet*, *JCAP* **09** (2021) 011 [[2012.12847](#)].
- [31] N. Benincasa, L. Delle Rose, K. Kannike and L. Marzola, *Multi-step phase transitions and gravitational waves in the inert doublet model*, *JCAP* **12** (2022) 025 [[2205.06669](#)].
- [32] A. Paul, D. Majumdar and B. Banerjee, *Gravitational Wave Signatures from First-Order Phase Transitions in an Extended Inert Doublet Dark Matter Model*, *Springer Proc. Phys.* **277** (2022) 73.

- [33] S. Jiang, F. P. Huang and X. Wang, *Bubble wall velocity during electroweak phase transition in the inert doublet model*, *Phys. Rev. D* **107** (2023) 095005 [2211.13142].
- [34] M. D. Astros, S. Fabian and F. Goertz, *Minimal Inert Doublet benchmark for dark matter and the baryon asymmetry*, *JCAP* **02** (2024) 052 [2307.01270].
- [35] N. Benincasa, A. Hryczuk, K. Kannike and M. Laletin, *Phase transitions and gravitational waves in a model of  $\mathbb{Z}_3$  scalar dark matter*, *JHEP* **02** (2024) 207 [2312.04627].
- [36] M. Carena, M. Quiros and C. E. M. Wagner, *Opening the window for electroweak baryogenesis*, *Phys. Lett. B* **380** (1996) 81 [hep-ph/9603420].
- [37] J. R. Espinosa, *Dominant two loop corrections to the MSSM finite temperature effective potential*, *Nucl. Phys. B* **475** (1996) 273 [hep-ph/9604320].
- [38] D. Delepine, J. M. Gerard, R. Gonzalez Felipe and J. Weyers, *A Light stop and electroweak baryogenesis*, *Phys. Lett. B* **386** (1996) 183 [hep-ph/9604440].
- [39] J. M. Cline and K. Kainulainen, *Supersymmetric electroweak phase transition: Beyond perturbation theory*, *Nucl. Phys. B* **482** (1996) 73 [hep-ph/9605235].
- [40] M. Losada, *High temperature dimensional reduction of the MSSM and other multiscalar models*, *Phys. Rev. D* **56** (1997) 2893 [hep-ph/9605266].
- [41] M. Laine, *Effective theories of MSSM at high temperature*, *Nucl. Phys. B* **481** (1996) 43 [hep-ph/9605283].
- [42] D. Bodeker, P. John, M. Laine and M. G. Schmidt, *The Two loop MSSM finite temperature effective potential with stop condensation*, *Nucl. Phys. B* **497** (1997) 387 [hep-ph/9612364].
- [43] B. de Carlos and J. R. Espinosa, *The Baryogenesis window in the MSSM*, *Nucl. Phys. B* **503** (1997) 24 [hep-ph/9703212].
- [44] J. M. Cline and G. D. Moore, *Supersymmetric electroweak phase transition: Baryogenesis versus experimental constraints*, *Phys. Rev. Lett.* **81** (1998) 3315 [hep-ph/9806354].
- [45] M. Losada, *The Two loop finite temperature effective potential of the MSSM and baryogenesis*, *Nucl. Phys. B* **537** (1999) 3 [hep-ph/9806519].
- [46] M. Laine and K. Rummukainen, *Two Higgs doublet dynamics at the electroweak phase transition: A Nonperturbative study*, *Nucl. Phys. B* **597** (2001) 23 [hep-lat/0009025].
- [47] M. Carena, G. Nardini, M. Quiros and C. E. M. Wagner, *The Baryogenesis Window in the MSSM*, *Nucl. Phys. B* **812** (2009) 243 [0809.3760].
- [48] A. Delgado, G. Nardini and M. Quiros, *The Light Stop Scenario from Gauge Mediation*, *JHEP* **04** (2012) 137 [1201.5164].
- [49] M. Carena, G. Nardini, M. Quiros and C. E. M. Wagner, *MSSM Electroweak Baryogenesis and LHC Data*, *JHEP* **02** (2013) 001 [1207.6330].
- [50] D. J. H. Chung, A. J. Long and L.-T. Wang, *125 GeV Higgs boson and electroweak phase transition model classes*, *Phys. Rev. D* **87** (2013) 023509 [1209.1819].
- [51] W. Huang, J. Shu and Y. Zhang, *On the Higgs Fit and Electroweak Phase Transition*, *JHEP* **03** (2013) 164 [1210.0906].
- [52] M. Laine, G. Nardini and K. Rummukainen, *Lattice study of an electroweak phase transition at  $m_h \simeq 126$  GeV*, *JCAP* **01** (2013) 011 [1211.7344].
- [53] S. Liebler, S. Profumo and T. Stefaniak, *Light Stop Mass Limits from Higgs Rate Measurements in the MSSM: Is MSSM Electroweak Baryogenesis Still Alive After All?*, *JHEP* **04** (2016) 143 [1512.09172].
- [54] H. H. Patel and M. J. Ramsey-Musolf, *Stepping Into Electroweak Symmetry Breaking: Phase Transitions and Higgs Phenomenology*, *Phys. Rev. D* **88** (2013) 035013 [1212.5652].

- [55] M. Chala, M. Ramos and M. Spannowsky, *Gravitational wave and collider probes of a triplet Higgs sector with a low cutoff*, *Eur. Phys. J. C* **79** (2019) 156 [[1812.01901](#)].
- [56] S. Baum, M. Carena, N. R. Shah, C. E. M. Wagner and Y. Wang, *Nucleation is more than critical: A case study of the electroweak phase transition in the NMSSM*, *JHEP* **03** (2021) 055 [[2009.10743](#)].
- [57] M. J. Kazemi and S. S. Abdussalam, *Electroweak Phase Transition in an Inert Complex Triplet Model*, *Phys. Rev. D* **103** (2021) 075012 [[2103.00212](#)].
- [58] I. Baldes, S. Blasi, A. Mariotti, A. Sevrin and K. Turbang, *Baryogenesis via relativistic bubble expansion*, *Phys. Rev. D* **104** (2021) 115029 [[2106.15602](#)].
- [59] A. Azatov, M. Vanvlasselaer and W. Yin, *Baryogenesis via relativistic bubble walls*, *JHEP* **10** (2021) 043 [[2106.14913](#)].
- [60] M. Jiang, L. Bian, W. Huang and J. Shu, *Impact of a complex singlet: Electroweak baryogenesis and dark matter*, *Phys. Rev. D* **93** (2016) 065032 [[1502.07574](#)].
- [61] C.-W. Chiang, M. J. Ramsey-Musolf and E. Senaha, *Standard Model with a Complex Scalar Singlet: Cosmological Implications and Theoretical Considerations*, *Phys. Rev. D* **97** (2018) 015005 [[1707.09960](#)].
- [62] A. Ahriche, K. Hashino, S. Kanemura and S. Nasri, *Gravitational Waves from Phase Transitions in Models with Charged Singlets*, *Phys. Lett. B* **789** (2019) 119 [[1809.09883](#)].
- [63] N. Chen, T. Li, Y. Wu and L. Bian, *Complementarity of the future  $e^+e^-$  colliders and gravitational waves in the probe of complex singlet extension to the standard model*, *Phys. Rev. D* **101** (2020) 075047 [[1911.05579](#)].
- [64] G.-C. Cho, C. Idegawa and E. Senaha, *Electroweak phase transition in a complex singlet extension of the Standard Model with degenerate scalars*, *Phys. Lett. B* **823** (2021) 136787 [[2105.11830](#)].
- [65] P. Schicho, T. V. I. Tenkanen and G. White, *Combining thermal resummation and gauge invariance for electroweak phase transition*, *JHEP* **11** (2022) 047 [[2203.04284](#)].
- [66] P. Di Bari and M. H. Rahat, *The split majoron model confronts the NANOGrav signal*, [2307.03184](#).
- [67] J. R. Espinosa and M. Quiros, *The Electroweak phase transition with a singlet*, *Phys. Lett. B* **305** (1993) 98 [[hep-ph/9301285](#)].
- [68] S. Profumo, M. J. Ramsey-Musolf and G. Shaughnessy, *Singlet Higgs phenomenology and the electroweak phase transition*, *JHEP* **08** (2007) 010 [[0705.2425](#)].
- [69] J. M. Cline, G. Laporte, H. Yamashita and S. Kraml, *Electroweak Phase Transition and LHC Signatures in the Singlet Majoron Model*, *JHEP* **07** (2009) 040 [[0905.2559](#)].
- [70] J. M. Cline and K. Kainulainen, *Electroweak baryogenesis and dark matter from a singlet Higgs*, *JCAP* **01** (2013) 012 [[1210.4196](#)].
- [71] J. M. Cline, K. Kainulainen, P. Scott and C. Weniger, *Update on scalar singlet dark matter*, *Phys. Rev. D* **88** (2013) 055025 [[1306.4710](#)].
- [72] A. Katz and M. Perelstein, *Higgs Couplings and Electroweak Phase Transition*, *JHEP* **07** (2014) 108 [[1401.1827](#)].
- [73] S. Profumo, M. J. Ramsey-Musolf, C. L. Wainwright and P. Winslow, *Singlet-catalyzed electroweak phase transitions and precision Higgs boson studies*, *Phys. Rev. D* **91** (2015) 035018 [[1407.5342](#)].
- [74] V. Vaskonen, *Electroweak baryogenesis and gravitational waves from a real scalar singlet*, *Phys. Rev. D* **95** (2017) 123515 [[1611.02073](#)].

- [75] K. Hashino, M. Kakizaki, S. Kanemura, P. Ko and T. Matsui, *Gravitational waves and Higgs boson couplings for exploring first order phase transition in the model with a singlet scalar field*, *Phys. Lett. B* **766** (2017) 49 [1609.00297].
- [76] W. Chao, H.-K. Guo and J. Shu, *Gravitational Wave Signals of Electroweak Phase Transition Triggered by Dark Matter*, *JCAP* **09** (2017) 009 [1702.02698].
- [77] T. Matsui, *Gravitational waves from the first order electroweak phase transition in the  $Z_3$  symmetric singlet scalar model*, *EPJ Web Conf.* **168** (2018) 05001 [1709.05900].
- [78] Z. Kang, P. Ko and T. Matsui, *Strong first order EWPT & strong gravitational waves in  $Z_3$ -symmetric singlet scalar extension*, *JHEP* **02** (2018) 115 [1706.09721].
- [79] A. Alves, T. Ghosh, H.-K. Guo, K. Sinha and D. Vagie, *Collider and Gravitational Wave Complementarity in Exploring the Singlet Extension of the Standard Model*, *JHEP* **04** (2019) 052 [1812.09333].
- [80] V. R. Shajiee and A. Tofghi, *Electroweak Phase Transition, Gravitational Waves and Dark Matter in Two Scalar Singlet Extension of The Standard Model*, *Eur. Phys. J. C* **79** (2019) 360 [1811.09807].
- [81] A. Beniwal, M. Lewicki, M. White and A. G. Williams, *Gravitational waves and electroweak baryogenesis in a global study of the extended scalar singlet model*, *JHEP* **02** (2019) 183 [1810.02380].
- [82] T. Matsui, *Gravitational waves from the first order electroweak phase transition in the  $Z_3$  symmetric singlet scalar model*, *PoS CORFU2017* (2018) 092.
- [83] K. Kannike, K. Loos and M. Raidal, *Gravitational wave signals of pseudo-Goldstone dark matter in the  $Z_3$  complex singlet model*, *Phys. Rev. D* **101** (2020) 035001 [1907.13136].
- [84] S. Demidov, D. Gorbunov and E. Kriukova, *Gravitational waves from first-order electroweak phase transition in a model with light sgoldstones*, *JHEP* **07** (2022) 061 [2112.06083].
- [85] J. M. Cline, A. Friedlander, D.-M. He, K. Kainulainen, B. Laurent and D. Tucker-Smith, *Baryogenesis and gravity waves from a UV-completed electroweak phase transition*, *Phys. Rev. D* **103** (2021) 123529 [2102.12490].
- [86] Q.-H. Cao, K. Hashino, X.-X. Li and J.-H. Yue, *Multi-step phase transition and gravitational wave from general  $Z_2$  scalar extensions*, **2212.07756**.
- [87] P. Athron, C. Balázs, A. Fowlie, L. Morris and L. Wu, *Cosmological phase transitions: From perturbative particle physics to gravitational waves*, *Prog. Part. Nucl. Phys.* **135** (2024) 104094 [2305.02357].
- [88] T. Alanne, N. Benincasa, M. Heikinheimo, K. Kannike, V. Keus, N. Koivunen et al., *Pseudo-Goldstone dark matter: gravitational waves and direct-detection blind spots*, *JHEP* **10** (2020) 080 [2008.09605].
- [89] L. Bian, Y. Wu and K.-P. Xie, *Electroweak phase transition with composite Higgs models: calculability, gravitational waves and collider searches*, *JHEP* **12** (2019) 028 [1909.02014].
- [90] K.-P. Xie, L. Bian and Y. Wu, *Electroweak baryogenesis and gravitational waves in a composite Higgs model with high dimensional fermion representations*, *JHEP* **12** (2020) 047 [2005.13552].
- [91] C. Grojean, G. Servant and J. D. Wells, *First-order electroweak phase transition in the standard model with a low cutoff*, *Phys. Rev. D* **71** (2005) 036001 [hep-ph/0407019].
- [92] D. Bodeker, L. Fromme, S. J. Huber and M. Seniuch, *The Baryon asymmetry in the standard model with a low cut-off*, *JHEP* **02** (2005) 026 [hep-ph/0412366].
- [93] C. Delaunay, C. Grojean and J. D. Wells, *Dynamics of Non-renormalizable Electroweak Symmetry Breaking*, *JHEP* **04** (2008) 029 [0711.2511].

- [94] C. Balazs, G. White and J. Yue, *Effective field theory, electric dipole moments and electroweak baryogenesis*, *JHEP* **03** (2017) 030 [[1612.01270](#)].
- [95] J. de Vries, M. Postma, J. van de Vis and G. White, *Electroweak Baryogenesis and the Standard Model Effective Field Theory*, *JHEP* **01** (2018) 089 [[1710.04061](#)].
- [96] J. De Vries, M. Postma and J. van de Vis, *The role of leptons in electroweak baryogenesis*, *JHEP* **04** (2019) 024 [[1811.11104](#)].
- [97] M. Chala, C. Krause and G. Nardini, *Signals of the electroweak phase transition at colliders and gravitational wave observatories*, *JHEP* **07** (2018) 062 [[1802.02168](#)].
- [98] S. A. R. Ellis, S. Ipek and G. White, *Electroweak Baryogenesis from Temperature-Varying Couplings*, *JHEP* **08** (2019) 002 [[1905.11994](#)].
- [99] M. Postma and G. White, *Cosmological phase transitions: is effective field theory just a toy?*, *JHEP* **03** (2021) 280 [[2012.03953](#)].
- [100] B. Batell, A. Ghalsasi, M. Low and M. Rai, *Gravitational Waves from Naturalness*, *JHEP* **01** (2024) 148 [[2310.06905](#)].
- [101] T. Ghosh, A. Ghoshal, H.-K. Guo, F. Hajkarim, S. F. King, K. Sinha et al., *Did we hear the sound of the Universe boiling? Analysis using the full fluid velocity profiles and NANOGrav 15-year data*, [2307.02259](#).
- [102] P. Schwaller, *Gravitational Waves from a Dark Phase Transition*, *Phys. Rev. Lett.* **115** (2015) 181101 [[1504.07263](#)].
- [103] I. Baldes and C. Garcia-Cely, *Strong gravitational radiation from a simple dark matter model*, *JHEP* **05** (2019) 190 [[1809.01198](#)].
- [104] M. Breitbach, J. Kopp, E. Madge, T. Opferkuch and P. Schwaller, *Dark, Cold, and Noisy: Constraining Secluded Hidden Sectors with Gravitational Waves*, *JCAP* **07** (2019) 007 [[1811.11175](#)].
- [105] D. Croon, V. Sanz and G. White, *Model Discrimination in Gravitational Wave spectra from Dark Phase Transitions*, *JHEP* **08** (2018) 203 [[1806.02332](#)].
- [106] E. Hall, T. Konstandin, R. McGehee, H. Murayama and G. Servant, *Baryogenesis From a Dark First-Order Phase Transition*, *JHEP* **04** (2020) 042 [[1910.08068](#)].
- [107] I. Baldes, *Gravitational waves from the asymmetric-dark-matter generating phase transition*, *JCAP* **05** (2017) 028 [[1702.02117](#)].
- [108] D. Croon, A. Kusenko, A. Mazumdar and G. White, *Solitonsynthesis and Gravitational Waves*, *Phys. Rev. D* **101** (2020) 085010 [[1910.09562](#)].
- [109] E. Hall, T. Konstandin, R. McGehee and H. Murayama, *Asymmetric matter from a dark first-order phase transition*, *Phys. Rev. D* **107** (2023) 055011 [[1911.12342](#)].
- [110] W. Chao, X.-F. Li and L. Wang, *Filtered pseudo-scalar dark matter and gravitational waves from first order phase transition*, *JCAP* **06** (2021) 038 [[2012.15113](#)].
- [111] J. B. Dent, B. Dutta, S. Ghosh, J. Kumar and J. Runburg, *Sensitivity to dark sector scales from gravitational wave signatures*, *JHEP* **08** (2022) 300 [[2203.11736](#)].
- [112] A. J. Helmboldt, J. Kubo and S. van der Woude, *Observational prospects for gravitational waves from hidden or dark chiral phase transitions*, *Phys. Rev. D* **100** (2019) 055025 [[1904.07891](#)].
- [113] M. Aoki and J. Kubo, *Gravitational waves from chiral phase transition in a conformally extended standard model*, *JCAP* **04** (2020) 001 [[1910.05025](#)].
- [114] D. Croon, J. N. Howard, S. Ipek and T. M. P. Tait, *QCD baryogenesis*, *Phys. Rev. D* **101** (2020) 055042 [[1911.01432](#)].

- [115] D. Croon, R. Houtz and V. Sanz, *Dynamical Axions and Gravitational Waves*, *JHEP* **07** (2019) 146 [[1904.10967](#)].
- [116] J. Garcia-Bellido, H. Murayama and G. White, *Exploring the early Universe with Gaia and Theia*, *JCAP* **12** (2021) 023 [[2104.04778](#)].
- [117] W.-C. Huang, M. Reichert, F. Sannino and Z.-W. Wang, *Testing the dark  $SU(N)$  Yang-Mills theory confined landscape: From the lattice to gravitational waves*, *Phys. Rev. D* **104** (2021) 035005 [[2012.11614](#)].
- [118] J. Halverson, C. Long, A. Maiti, B. Nelson and G. Salinas, *Gravitational waves from dark Yang-Mills sectors*, *JHEP* **05** (2021) 154 [[2012.04071](#)].
- [119] Z. Kang, J. Zhu and S. Matsuzaki, *Dark confinement-deconfinement phase transition: a roadmap from Polyakov loop models to gravitational waves*, *JHEP* **09** (2021) 060 [[2101.03795](#)].
- [120] B. Fornal and E. Pierre, *Asymmetric dark matter from gravitational waves*, *Phys. Rev. D* **106** (2022) 115040 [[2209.04788](#)].
- [121] F. Costa, S. Khan and J. Kim, *A two-component dark matter model and its associated gravitational waves*, *JHEP* **06** (2022) 026 [[2202.13126](#)].
- [122] K. Hashino, M. Kakizaki, S. Kanemura, P. Ko and T. Matsui, *Gravitational waves from first order electroweak phase transition in models with the  $U(1)_X$  gauge symmetry*, *JHEP* **06** (2018) 088 [[1802.02947](#)].
- [123] F. P. Huang and X. Zhang, *Probing the gauge symmetry breaking of the early universe in 3-3-1 models and beyond by gravitational waves*, *Phys. Lett. B* **788** (2019) 288 [[1701.04338](#)].
- [124] D. Croon, T. E. Gonzalo and G. White, *Gravitational Waves from a Pati-Salam Phase Transition*, *JHEP* **02** (2019) 083 [[1812.02747](#)].
- [125] V. Brdar, L. Graf, A. J. Helmboldt and X.-J. Xu, *Gravitational Waves as a Probe of Left-Right Symmetry Breaking*, *JCAP* **12** (2019) 027 [[1909.02018](#)].
- [126] W.-C. Huang, F. Sannino and Z.-W. Wang, *Gravitational Waves from Pati-Salam Dynamics*, *Phys. Rev. D* **102** (2020) 095025 [[2004.02332](#)].
- [127] B. Fornal, K. Garcia and E. Pierre, *Testing unification and dark matter with gravitational waves*, *Phys. Rev. D* **108** (2023) 055022 [[2305.12566](#)].
- [128] P. Costa, C. A. de Sousa, M. C. Ruivo and H. Hansen, *The QCD critical end point in the PNJL model*, *EPL* **86** (2009) 31001 [[0801.3616](#)].
- [129] F. Marquez and R. Zamora, *Critical end point in a thermomagnetic nonlocal NJL model*, *Int. J. Mod. Phys. A* **32** (2017) 1750162 [[1702.04161](#)].
- [130] V. Vovchenko, M. I. Gorenstein, C. Greiner and H. Stoecker, *Hagedorn bag-like model with a crossover transition meets lattice QCD*, *Phys. Rev. C* **99** (2019) 045204 [[1811.05737](#)].
- [131] R. Câmara Pereira, J. a. Moreira and P. Costa, *The strange critical endpoint and isentropic trajectories in an extended PNJL model with eight Quark interactions*, *Eur. Phys. J. A* **56** (2020) 214 [[2006.02385](#)].
- [132] F. Gao and J. M. Pawłowski, *QCD phase structure from functional methods*, *Phys. Rev. D* **102** (2020) 034027 [[2002.07500](#)].
- [133] F. Gao and J. M. Pawłowski, *Chiral phase structure and critical end point in QCD*, *Phys. Lett. B* **820** (2021) 136584 [[2010.13705](#)].
- [134] F. Gao and I. M. Oldengott, *Cosmology Meets Functional QCD: First-Order Cosmic QCD Transition Induced by Large Lepton Asymmetries*, *Phys. Rev. Lett.* **128** (2022) 131301 [[2106.11991](#)].

- [135] F. Gao, J. Harz, C. Hati, Y. Lu, I. M. Oldengott and G. White, *Sphaleron freeze-in baryogenesis with gravitational waves from the QCD transition*, [2309.00672](#).
- [136] F. Bigazzi, A. Caddeo, A. L. Cotrone and A. Paredes, *Fate of false vacua in holographic first-order phase transitions*, *JHEP* **12** (2020) 200 [[2008.02579](#)].
- [137] F. Bigazzi, A. Caddeo, A. L. Cotrone and A. Paredes, *Dark Holograms and Gravitational Waves*, *JHEP* **04** (2021) 094 [[2011.08757](#)].
- [138] X. Wang, F. P. Huang and X. Zhang, *Bubble wall velocity beyond leading-log approximation in electroweak phase transition*, [2011.12903](#).
- [139] E. Morgante, N. Ramberg and P. Schwaller, *Gravitational waves from dark  $SU(3)$  Yang-Mills theory*, *Phys. Rev. D* **107** (2023) 036010 [[2210.11821](#)].
- [140] M. Hindmarsh, *Sound shell model for acoustic gravitational wave production at a first-order phase transition in the early Universe*, *Phys. Rev. Lett.* **120** (2018) 071301 [[1608.04735](#)].
- [141] M. Hindmarsh and M. Hijazi, *Gravitational waves from first order cosmological phase transitions in the Sound Shell Model*, *JCAP* **12** (2019) 062 [[1909.10040](#)].
- [142] H.-K. Guo, K. Sinha, D. Vagie and G. White, *Phase Transitions in an Expanding Universe: Stochastic Gravitational Waves in Standard and Non-Standard Histories*, *JCAP* **01** (2021) 001 [[2007.08537](#)].
- [143] D. Cutting, M. Hindmarsh and D. J. Weir, *Gravitational waves from vacuum first-order phase transitions: from the envelope to the lattice*, *Phys. Rev. D* **97** (2018) 123513 [[1802.05712](#)].
- [144] D. Cutting, E. G. Escartin, M. Hindmarsh and D. J. Weir, *Gravitational waves from vacuum first order phase transitions II: from thin to thick walls*, *Phys. Rev. D* **103** (2021) 023531 [[2005.13537](#)].
- [145] O. Gould, S. Sukuvaara and D. Weir, *Vacuum bubble collisions: From microphysics to gravitational waves*, *Phys. Rev. D* **104** (2021) 075039 [[2107.05657](#)].
- [146] D. J. Weir, *Gravitational waves from a first order electroweak phase transition: a brief review*, *Phil. Trans. Roy. Soc. Lond. A* **376** (2018) 20170126 [[1705.01783](#)].
- [147] C. Gowling and M. Hindmarsh, *Observational prospects for phase transitions at LISA: Fisher matrix analysis*, *JCAP* **10** (2021) 039 [[2106.05984](#)].
- [148] C. Gowling, M. Hindmarsh, D. C. Hooper and J. Torrado, *Reconstructing physical parameters from template gravitational wave spectra at LISA: first order phase transitions*, *JCAP* **04** (2023) 061 [[2209.13551](#)].
- [149] F. Giese, T. Konstandin and J. van de Vis, *Finding sound shells in LISA mock data using likelihood sampling*, *JCAP* **11** (2021) 002 [[2107.06275](#)].
- [150] P. Athron, C. Balázs, T. E. Gonzalo and M. Pearce, *Falsifying Pati-Salam models with LIGO*, *Phys. Rev. D* **109** (2024) L061303 [[2307.02544](#)].
- [151] R. Roshan and G. White, *Using gravitational waves to see the first second of the Universe*, [2401.04388](#).
- [152] A. Mazumdar and G. White, *Review of cosmic phase transitions: their significance and experimental signatures*, *Rept. Prog. Phys.* **82** (2019) 076901 [[1811.01948](#)].
- [153] M. Hindmarsh, S. J. Huber, K. Rummukainen and D. J. Weir, *Gravitational waves from the sound of a first order phase transition*, *Phys. Rev. Lett.* **112** (2014) 041301 [[1304.2433](#)].
- [154] M. Hindmarsh, S. J. Huber, K. Rummukainen and D. J. Weir, *Numerical simulations of acoustically generated gravitational waves at a first order phase transition*, *Phys. Rev. D* **92** (2015) 123009 [[1504.03291](#)].

- [155] J. R. Espinosa, T. Konstandin, J. M. No and G. Servant, *Energy Budget of Cosmological First-order Phase Transitions*, *JCAP* **06** (2010) 028 [[1004.4187](#)].
- [156] C. Caprini, R. Durrer and G. Servant, *The stochastic gravitational wave background from turbulence and magnetic fields generated by a first-order phase transition*, *JCAP* **12** (2009) 024 [[0909.0622](#)].
- [157] M. Hindmarsh, S. J. Huber, K. Rummukainen and D. J. Weir, *Shape of the acoustic gravitational wave power spectrum from a first order phase transition*, *Phys. Rev. D* **96** (2017) 103520 [[1704.05871](#)].
- [158] H.-K. Guo, K. Sinha, D. Vagie and G. White, *The benefits of diligence: how precise are predicted gravitational wave spectra in models with phase transitions?*, *JHEP* **06** (2021) 164 [[2103.06933](#)].
- [159] F. Giese, T. Konstandin, K. Schmitz and J. van de Vis, *Model-independent energy budget for LISA*, *JCAP* **01** (2021) 072 [[2010.09744](#)].
- [160] T. Krajewski, M. Lewicki and M. Zych, *Bubble-wall velocity in local thermal equilibrium: hydrodynamical simulations vs analytical treatment*, [2402.15408](#).
- [161] S. J. Huber and T. Konstandin, *Gravitational Wave Production by Collisions: More Bubbles*, *JCAP* **09** (2008) 022 [[0806.1828](#)].
- [162] J. Ellis, M. Lewicki and J. M. No, *Gravitational waves from first-order cosmological phase transitions: lifetime of the sound wave source*, *JCAP* **07** (2020) 050 [[2003.07360](#)].
- [163] D. Cutting, M. Hindmarsh and D. J. Weir, *Vorticity, kinetic energy, and suppressed gravitational wave production in strong first order phase transitions*, *Phys. Rev. Lett.* **125** (2020) 021302 [[1906.00480](#)].
- [164] M. Drees, F. Hajkarim and E. R. Schmitz, *The Effects of QCD Equation of State on the Relic Density of WIMP Dark Matter*, *JCAP* **06** (2015) 025 [[1503.03513](#)].
- [165] A. Roper Pol, S. Procacci and C. Caprini, *Characterization of the gravitational wave spectrum from sound waves within the sound shell model*, [2308.12943](#).
- [166] A. Roper Pol, A. Neronov, C. Caprini, T. Boyer and D. Semikoz, *LISA and  $\gamma$ -ray telescopes as multi-messenger probes of a first-order cosmological phase transition*, [2307.10744](#).
- [167] R. Sharma, J. Dahl, A. Brandenburg and M. Hindmarsh, *Shallow relic gravitational wave spectrum with acoustic peak*, *JCAP* **12** (2023) 042 [[2308.12916](#)].
- [168] K. Schmitz, *New Sensitivity Curves for Gravitational-Wave Signals from Cosmological Phase Transitions*, *JHEP* **01** (2021) 097 [[2002.04615](#)].
- [169] R. Jinno, T. Konstandin, H. Rubira and J. van de Vis, *Effect of density fluctuations on gravitational wave production in first-order phase transitions*, *JCAP* **12** (2021) 019 [[2108.11947](#)].
- [170] H.-K. Guo, *Dissipative Effects as New Observables for Cosmological Phase Transitions*, [2310.10927](#).